



AN ABSTRACT OF THE THESIS OF

Janakiram Ganesh Sankaranarayanan for the degree of Master of Science in  
Electrical and Computer Engineering presented on June 17, 2005.

Title: Modeling and Simulation Methods for RF MEMS VCOs

Abstract approved: \_\_\_\_\_

Kartikeya Mayaram

This work focusses on the modeling and the development of efficient coupled simulation techniques for MEMS based RF oscillators. High-level models for MEMS based varactors have been discussed and their accuracy issues are identified, based on comparisons with numerical simulations. A faster simulation approach based on the time-domain shooting method is proposed for computation of the steady state in MEMS based oscillators. Analysis, simulation and modeling techniques to characterize the effect of mechanical noise on the phase noise performance of these VCOs is presented.

©Copyright by Janakiram Ganesh Sankaranarayanan

June 17, 2005

All Rights Reserved

Modeling and Simulation Methods for RF MEMS VCOs

by

Janakiram Ganesh Sankaranarayanan

A THESIS

submitted to

Oregon State University

in partial fulfillment of  
the requirements for the  
degree of

Master of Science

Presented June 17, 2005  
Commencement June 2006

Master of Science thesis of Janakiram Ganesh Sankaranarayanan presented on  
June 17, 2005

APPROVED:

---

Major Professor, representing Electrical and Computer Engineering

---

Associate director of the School of Electrical Engineering and Computer Science

---

Dean of the Graduate School

I understand that my thesis will become part of the permanent collection of Oregon State University libraries. My signature below authorizes release of my thesis to any reader upon request.

---

Janakiram Ganesh Sankaranarayanan, Author

## ACKNOWLEDGEMENTS

I would like to acknowledge NSF for their financial support which has made this work possible.

I would like to thank my research advisor Dr. Karti Mayaram for his patience and support during the course of this work. His valuable guidance helped me to do some systematic and methodical research. The courses I learnt under him, provided good foundation in analog/RF design and simulation.

I thank Dr. Un Ku Moon, Dr. Huaping Liu and Dr. Keith Levien for serving on my committee. Dr. Moon's courses helped me hone my knowledge in analog circuit design.

I wish to express my sincere gratitude to Dr. Mani Subramanian for his invaluable support during my initial course of study. I also take this opportunity to acknowledge Dr. Vincenzo Peluso of Qualcomm for his valuable advice during the course of my internship.

My special thanks goes to Manas Behera now with Epoch MicroElectronics for all the technical and non-technical help. I also benefitted a lot from the technical discussions with Volodymr Kratyuk. Sudipto of Beckman Institute of Advanced Science and Technology, UIUC was extremely helpful. My sincere thanks to the other members of my group Yutao (now with Agilent), Vijay, Maneesha, Igor, Xiaochuan for their support.

I would like to thank my labmates Moski, Sasi, Manu, Laddu, Ashok and other friends for their help and support. Many thanks to all my roommates who had made my stay at OSU memorable.

My sincere gratitude to appa, amma, periappa for all their blessings and support. My brother Sundar, has been a source of encouragement and provided guidance when I needed it the most.

To Amma, Appa, Periappa and Sundar

## TABLE OF CONTENTS

	<u>Page</u>
1 INTRODUCTION .....	1
1.1 Background and Motivation .....	1
1.2 Prior Work .....	2
1.3 Contributions .....	3
1.4 Thesis Organization .....	4
2 ACCURACY ISSUES IN HIGH LEVEL MODELS OF MEMS VARAC- TORS.....	5
2.1 Introduction.....	5
2.2 Overview.....	5
2.2.1 Working principle .....	5
2.2.2 Mechanical characteristics .....	7
2.2.3 MEMS capacitor structures .....	9
2.2.3.1 Cantilever Beams and Fixed-Fixed Beams .....	9
2.2.3.2 Parallel Plate Capacitor with Suspension Structures ...	10
2.3 High-level Models .....	10
2.3.1 Equivalent circuit model .....	10
2.3.2 Behavioral model .....	13
2.4 Electrostatic/Numerical Solver .....	13
2.5 Results.....	15
2.5.1 VCO simulations .....	19
2.6 Summary.....	20
3 PERIODIC STEADY-STATE ANALYSIS OF RF MEMS VCOs .....	22
3.1 VCO Simulation Methods .....	22
3.1.1 Transient analysis .....	22

TABLE OF CONTENTS (Continued)

	<u>Page</u>
3.1.2	Periodic steady-state analysis . . . . . 23
3.2	Simulation Method for RF MEMS VCOs . . . . . 24
3.2.1	Dynamics . . . . . 24
3.2.2	Simulation approach . . . . . 25
3.3	Simulation of VCOs in COSMO . . . . . 28
3.3.1	Static simulation method . . . . . 28
3.3.2	Dynamic simulation method . . . . . 29
3.4	Simulation Results . . . . . 30
3.4.1	Comparison with transient simulation methods . . . . . 30
3.4.2	VCO simulations . . . . . 31
3.5	Summary . . . . . 31
4	PHASE NOISE IN MEMS VCOs . . . . . 33
4.1	Overview . . . . . 33
4.1.1	Mechanical noise . . . . . 33
4.1.2	Displacement noise power spectral density . . . . . 34
4.2	Brownian Motion Induced Phase Noise . . . . . 35
4.3	Noise Current Modeling . . . . . 36
4.4	Current Noise Power Spectral Density . . . . . 39
4.4.1	Noise contribution from term 1 . . . . . 39
4.4.2	Noise contribution from term 2 . . . . . 44
4.5	Phase Noise Calculation Technique . . . . . 46
4.5.1	Nonlinear perturbation analysis . . . . . 46
4.5.2	Simulating Brownian motion induced phase noise . . . . . 47

TABLE OF CONTENTS (Continued)

	<u>Page</u>
4.6 Equivalent Circuit Model for Brownian Noise.....	48
4.7 Simulation Results .....	51
4.8 Summary.....	55
5 CONCLUSIONS AND FUTURE WORK.....	56
BIBLIOGRAPHY .....	57
APPENDICES .....	59
APPENDIX A AHDL code.....	60
APPENDIX B Spice netlist .....	62

## LIST OF FIGURES

Figure	Page
1.1 Coupling methodology in COSMO. . . . .	2
2.1 Functional model of an electro-mechanically tunable parallel-plate capacitor with two parallel plates. . . . .	6
2.2 Mass spring damper model. . . . .	8
2.3 Frequency response of the displacement/input force transfer function. . . . .	8
2.4 Deformation in cantilever and fixed-fixed beams due to an applied voltage. . . . .	9
2.5 Top view and cross-sectional view of the two parallel plate capacitor. . . . .	11
2.6 Equivalent circuit model. . . . .	12
2.7 Equivalent circuit model in HSPICE. . . . .	12
2.8 Behavioral model. . . . .	13
2.9 Capacitance as a function of the stiffness constant. . . . .	15
2.10 C-V curves for different thicknesses. . . . .	16
2.11 C-V curve for parallel plate capacitor. . . . .	17
2.12 Displacement of (a) cantilever beam and (b) fixed-fixed beam. . . . .	18
2.13 C-V curve of (a) cantilever beam and (b) fixed-fixed beam. . . . .	18
2.14 C-V curve for different materials. . . . .	19
2.15 Voltage controlled oscillator. . . . .	20
2.16 VCO tuning characteristics. . . . .	21
3.1 Comparison between step and sinusoidal responses for a MEMS varactor. . . . .	26
3.2 Flowchart of simulation method. . . . .	27
3.3 VCO tuning characteristics from the static simulation and periodic steady-state methods. . . . .	31
4.1 Displacement noise power spectral density. . . . .	35
4.2 Brownian motion induced phase noise. . . . .	36

LIST OF FIGURES (Continued)

<u>Figure</u>	<u>Page</u>
4.3 Noise current model for the MEMS capacitor. . . . .	38
4.4 Noise model describing the conversion of Brownian noise into a noise current. . . . .	39
4.5 HPSDs of the time varying power spectral density. . . . .	43
4.6 Normalized current noise power spectral densities. . . . .	45
4.7 A RLC series circuit. . . . .	49
4.8 Equivalent circuit to model the displacement noise. . . . .	50
4.9 Behavioral-circuit model. . . . .	51
4.10 Output current noise of the equivalent circuit model. . . . .	51
4.11 Colpitts VCO. . . . .	52
4.12 Phase noise computed using different simulation approaches $Q_M=1\dots$	54
4.13 Phase noise computed using different simulation approaches for $Q_M=10$ .	54

(

# MODELING AND SIMULATION METHODS FOR RF MEMS VCOs

## 1. INTRODUCTION

### 1.1. Background and Motivation

The goal of the wireless industry is to lower the cost, power dissipation, weight and size of portable transceivers. With only a very small section of a transceiver operating in the RF range, the RF section continues to be a design bottleneck [1]. One of the primary reasons being the level of integration in RF sections is low compared to other types of integrated circuits [2]. RF circuits mainly require numerous off-chip components that are difficult to bring onto the chip even in modern fabrication processes [1]. Micro electro-mechanical technology, commonly referred to as micromachining technology offers a potential solution of integrating these off-chip components onto silicon substrates [3]. Band-pass filters at RF and IF, RF switches, MEMS based varactors in VCOs, through the use of this technology have resulted in a considerable reduction in size [3].

A crucial part in the design phase of such systems is the verification of their behavior by simulation. Although there are very sophisticated CAD tools for integrated circuits, these tools are not applicable to the design of micro electro-mechanical systems (MEMS) [4]. This is mainly due to the fact that MEMS based circuits require electrostatic/mechanical analysis to verify their behavior. Coupled simulation techniques can be employed to analyze MEMS based electronic circuits [5], [6]. Circuit simulators have analytical models for simulating circuit components. In the absence of accurate analytical models, a device level simulator provides the solution of device characteristics. This forms the basic idea of a coupled

device and circuit simulator. High-level models can also be used to simulate the electro-mechanical behavior of MEMS based devices [8]. This work investigates the application of coupled simulations and high-level modeling in verifying such systems, in particular, MEMS based oscillators.

## 1.2. Prior Work

A coupled circuit and device simulator for the simulation of RF MEMS VCOs (COSMO) was proposed in [6] and is extended in this work. COSMO is an integration of the circuit simulator SPICE3f5 with a device simulator EM8.9. EM8.9 is a numerical solver for electrostatic/mechanical MEMS analysis using a meshless method [10]. This section provides an overview of the coupling methodology in COSMO.

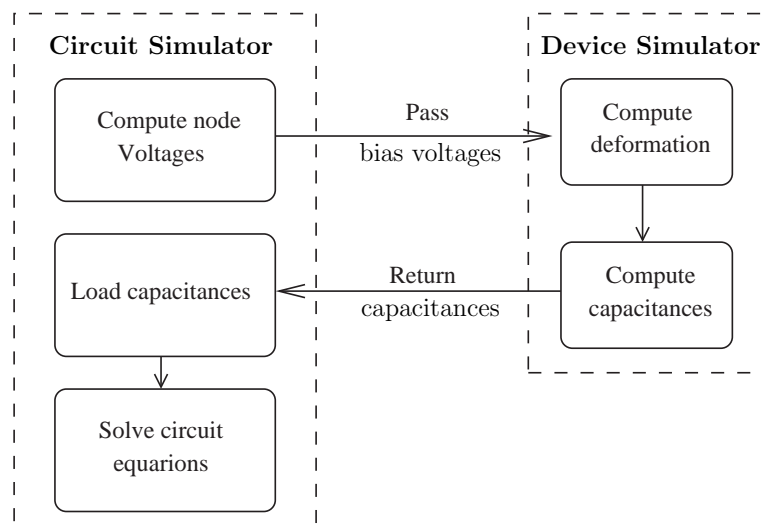


FIGURE 1.1. Coupling methodology in COSMO.

A MEMS based varactor undergoes mechanical deformation for a given input voltage. Based on the mechanical deformation, it presents a certain capacitance. EM8.9 solves for the structural deformation of the MEMS capacitors for a

given applied voltage. This solution obtained from EM8.9 is used to compute the capacitance of the MEMS capacitor. This capacitance is an input to SPICE3f5. Figure 1.1 illustrates the coupling methodology in COSMO.

In [8], high-level modeling of MEMS based varactors has been discussed. An equivalent circuit to model the electro-mechanical characteristics of MEMS varactors was also presented.

### 1.3. Contributions

High-level modeling trades off accuracy for speed. This work examines the accuracy issues and limitations of high-level models based on comparisons with coupled simulations.

A faster simulation approach to compute the steady state of RF MEMS VCOs is proposed. This method exploits the dynamic behavior of MEMS based varactors to reduce the number of device calls. In comparison with a full transient simulation, the proposed method shows a significant improvement in simulation time.

Phase noise is one of the important performance parameters in a VCO. In a RF MEMS VCO, in addition to the electrical noise, the mechanical noise from the MEMS devices contributes to the overall phase noise. This work mainly involves developing a theoretical framework to simulate phase noise in RF MEMS VCOs.

An equivalent circuit to model the mechanical noise in MEMS based varactors is developed. This model can be used with the high-level models for MEMS based varactors to simulate the phase noise in RF MEMS VCOs.

## 1.4. Thesis Organization

This thesis is organized into five chapters. Chapter 2 starts with a brief overview of the working principle of MEMS based varactors. It discusses two different macromodels for MEMS based varactors and compares their accuracy with numerical simulations in EM8.9.

Chapter 3 discusses a faster method of simulating RF MEMS VCOs based on periodic steady state methods. Comparisons are made with the existing simulation methods in terms of simulation time and number of device calls.

Chapter 4 presents theoretical analysis and simulation techniques to characterize the effect of mechanical noise in MEMS based varactors on the phase noise performance of RF MEMS VCOs. An equivalent circuit to model the mechanical noise in these devices is also developed.

Chapter 5 summarizes the outcome of this work and concludes with suggestions for future research.

## 2. ACCURACY ISSUES IN HIGH LEVEL MODELS OF MEMS VARACTORS

### 2.1. Introduction

Recent developments in micromachining technology have made possible the implementation of MEMS-based varactors. Compared with solid-state varactors, MEMS-based varactors have the advantages of lower loss and potentially greater tuning range. In addition to having a high Q factor and a wide tuning range, these devices can also withstand large voltage swings, thus making them suitable for low phase noise VCO applications [7]. An accurate way to simulate MEMS based VCOs is by using a coupled device and circuit simulator. Coupled simulations are time consuming and computationally expensive. Use of high-level models is a possibility when computational speed is more important than accuracy. For this reason, the accuracy issues of high-level models need to be determined. In this chapter, we compare two different methods for modeling the MEMS varactor structures. An equivalent circuit model [8] and a behavioral model are compared with numerical simulations from an electrostatic/mechanical solver EM8.9 [10]. Accuracy issues of the high-level models are identified in the context of RF MEMS VCOs.

### 2.2. Overview

#### 2.2.1. Working principle

The functional model of an electro-mechanically tunable capacitor shown in Figure 2.3 consists of two parallel plates. The top plate of the capacitor is suspended by a spring with spring constant  $k$ , while the bottom plate of the capacitor

is fixed. When a bias voltage is applied across the capacitor plates, the suspended plate is attracted towards the bottom plate due to the resultant electrostatic force. The suspended plate moves towards the fixed plate until equilibrium between the electrostatic and the spring forces is reached.

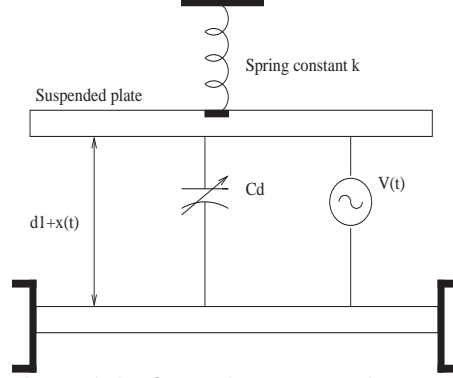


FIGURE 2.1. Functional model of an electro-mechanically tunable parallel-plate capacitor with two parallel plates.

Under DC conditions, at equilibrium, the electrostatic force and the spring force can be equated as given below (2.1)

$$kx = \frac{-0.5\epsilon_o AV^2}{(d_1 + x(V))^2} \quad (2.1)$$

where,  $\epsilon_o = 8.85415 \times 10^{-12}$  F/m is the dielectric constant of air,  $A$  is the area of the capacitor plates,  $d_1$  is the separation of the capacitor plates for no applied bias voltage,  $x$  is the displacement of the suspended plate,  $k$  is the spring constant and  $V$  is the applied voltage.

The parallel plate capacitance  $C_d$  is given by [8]

$$C_d(V) = \frac{\epsilon_o A}{(d_1 + x(V))} \quad (2.2)$$

It should be noted that the suspended plate will make contact with the bottom plate if the electrostatic force is greater than the spring force, which occurs when  $x < d_1/3$ . The voltage at which this occurs is called the pullin voltage [8].

Therefore, the maximum theoretical tuning range is 1.5:1. The pullin voltage is given by

$$V_{PI} = \sqrt{\frac{8kd^3}{27\epsilon_0 A}} \quad (2.3)$$

From the above equation it can be seen that for a given nominal capacitance the pull-in voltage depends only on the spring constant,  $k$ .

### 2.2.2. Mechanical characteristics

The MEMS capacitor can be modeled as a mass-spring-damper system as shown in Figure 2.2. There are two parallel plates, the top one is restrained by a spring and damper and the bottom plate is fixed. The spring represents the restoring force from the support of the top plate, while the damper represents the air resistance. With no applied bias the weight and the spring force on the top plate reach equilibrium. The damper has an effect only when the plate is in motion [11]. The dynamics of the electro-mechanical system can be described as follows

$$m \frac{d^2x}{dt^2} + r \frac{dx}{dt} + kx = F_e \quad (2.4)$$

where,  $m$  is the mass of the suspended plate,  $r$  is the mechanical resistance due to the surrounding gas ambient and the internal dissipation of the system, and  $F_e$  is the electrostatic driving force.

This linear equation can be transformed into the frequency domain and the transfer function between the force  $F_e$  and the displacement  $X(s)$  is given by

$$\frac{X(s)}{F_e(s)} = \frac{1/m}{s^2 + \frac{\omega_n}{Q_M} s + \frac{k}{m}} \quad (2.5)$$

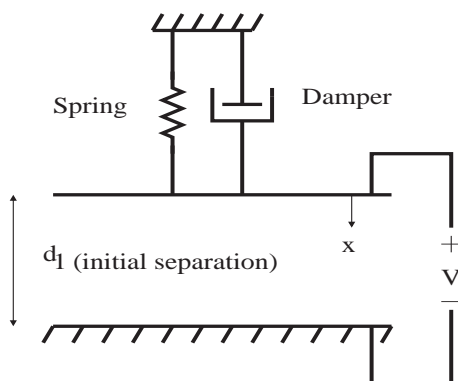


FIGURE 2.2. Mass spring damper model.

where the mechanical resonant frequency  $\omega_n = \sqrt{\frac{k}{m}}$  and  $Q_M = \frac{\omega_n m}{r}$ . Figure ?? shows the transfer function on a logarithmic scale. For frequencies above  $\omega_n$  the transfer function falls at 40 dB/decade. Hence the capacitor air gap is virtually constant for input force at frequencies much larger than  $\omega_n$ . There is a peaking in the transfer function at  $\omega_n$  which increases with higher values of  $Q_M$ . The MEMS

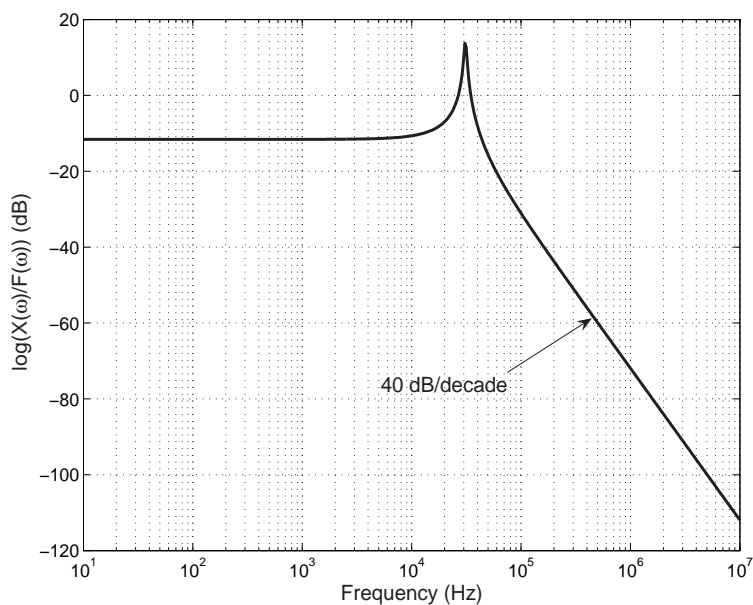


FIGURE 2.3. Frequency response of the displacement/input force transfer function.

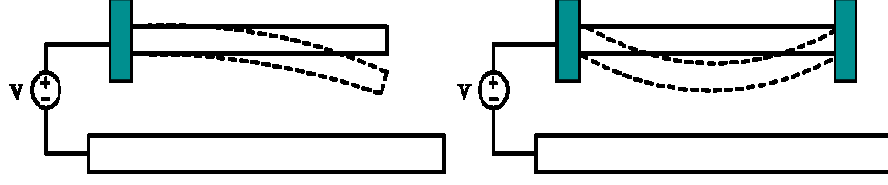


FIGURE 2.4. Deformation in cantilever and fixed-fixed beams due to an applied voltage.

electrostatic capacitor is voltage controlled. Hence the electrostatic driving force  $F_e$  is a function of the voltage. Substituting for  $F_e$  in (2.4),

$$m \frac{d^2x}{dt^2} + r \frac{dx}{dt} + kx = \frac{-0.5\epsilon_o AV^2(t)}{(d_1 + x(t))^2} \quad (2.6)$$

This equation is a second order non-linear differential equation that relates the applied voltage  $V$  with the displacement  $x$  in the capacitor.

### 2.2.3. MEMS capacitor structures

#### 2.2.3.1. Cantilever Beams and Fixed-Fixed Beams

Cantilever beams and fixed-fixed beams are the simplest forms of electrostatically actuated MEMS-based capacitor structures. These structures and their deformation due to the application of an external bias voltage are shown in Figure 2.4. The working principle of these capacitors is based on (2.1) where, the stiffness constant,  $k$ , for the cantilever beam capacitor and the fixed-fixed beam capacitor depend on the dimensions of the capacitor itself and are given in (2.7) and (2.8), respectively [11].

$$k_{cant} = \frac{2EW}{3} \left( \frac{t}{L} \right)^3 \quad (2.7)$$

and,

$$k_{fixed} = 32EW \left( \frac{t}{L} \right)^3 \quad (2.8)$$

where,  $E$  is the Young's modulus of the material of the capacitor, and  $W$ ,  $t$ ,  $L$  are the width, thickness, and length of the suspended plate, respectively.

### 2.2.3.2. Parallel Plate Capacitor with Suspension Structures

The top view of a MEMS based capacitor with suspension structures is shown in Figure 2.5. The suspension structures are designed to obtain the stiffness constant and thus the desired tuning range. The stiffness constant of a suspension structure with length  $L$ , width  $W$  and thickness  $t$  is given by (2.9) [8, 11]

$$k_{susp} = EW \left( \frac{t}{L} \right)^3 \quad (2.9)$$

From (2.9) it can be seen that the spring constant is linearly proportional to the beam width and highly dependent on the length and thickness of the beam. Therefore, by varying the dimension of the suspension structures, different beam stiffnesses can be obtained for various tuning voltages. The simulated structure had an equivalent spring constant of 44 N/m with a tuning voltage of 3.3 V. The length and width of the suspension structure were chosen as  $100\mu m$  and  $20\mu m$ , respectively.

## 2.3. High-level Models

### 2.3.1. Equivalent circuit model

The equivalent circuit model as presented in [8] for a tunable capacitor with two parallel plates is shown in Figure 2.6. The mechanical domain of the

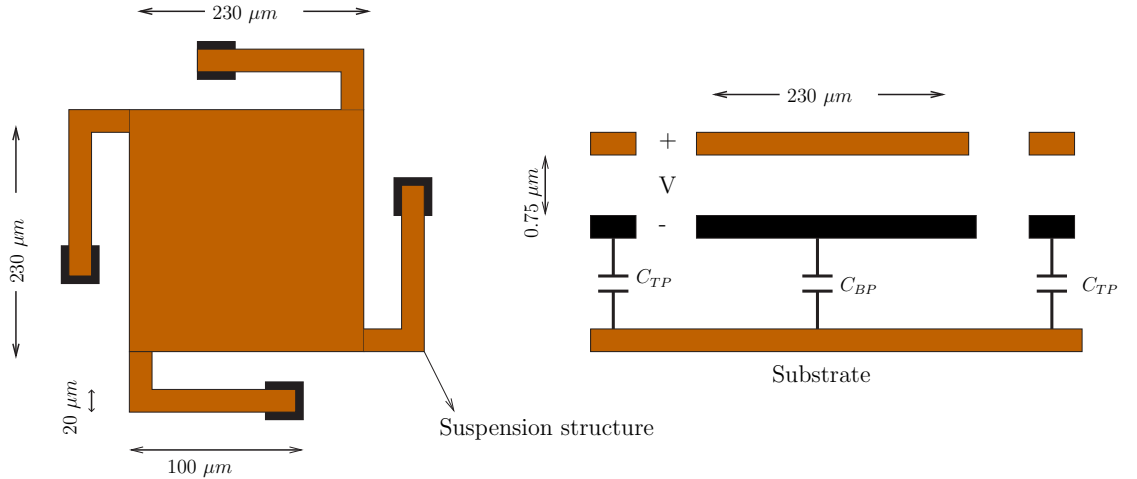


FIGURE 2.5. Top view and cross-sectional view of the two parallel plate capacitor.

model is based on (2.6) whose output is the displacement  $x(t)$ . The right-hand side term  $\frac{-0.5\epsilon_o AV^2(t)}{(d_1+x(t))^2}$  of (2.6) represents the electrostatic driving force and is modeled as a current source  $i_{IN}(t)$ . The mass,  $m$ , of the suspended plate is modeled as an equivalent capacitor while the mechanical resistance,  $r$ , is modeled as a resistor. The transconductor  $G_2$  and capacitor  $C_2$  integrate the voltage across this parallel  $RC$  combination to give the output  $x(t)$ . The spring constant  $k_m$  is modeled as an equivalent transconductor in negative feedback.

For an applied voltage the mechanical domain of the model gives the displacement  $x(t)$  as its output. The resultant current that flows through the capacitor is a function of this displacement and is given by (2.10)

$$i(t) = C(t) \frac{dV(t)}{dt} + V(t) \frac{dC(t)}{dt} \quad (2.10)$$

The electrical domain of the model represents the electrical characteristics of the MEMS variable capacitor. A voltage dependent capacitor and a current source is used to model the current through the MEMS capacitor.

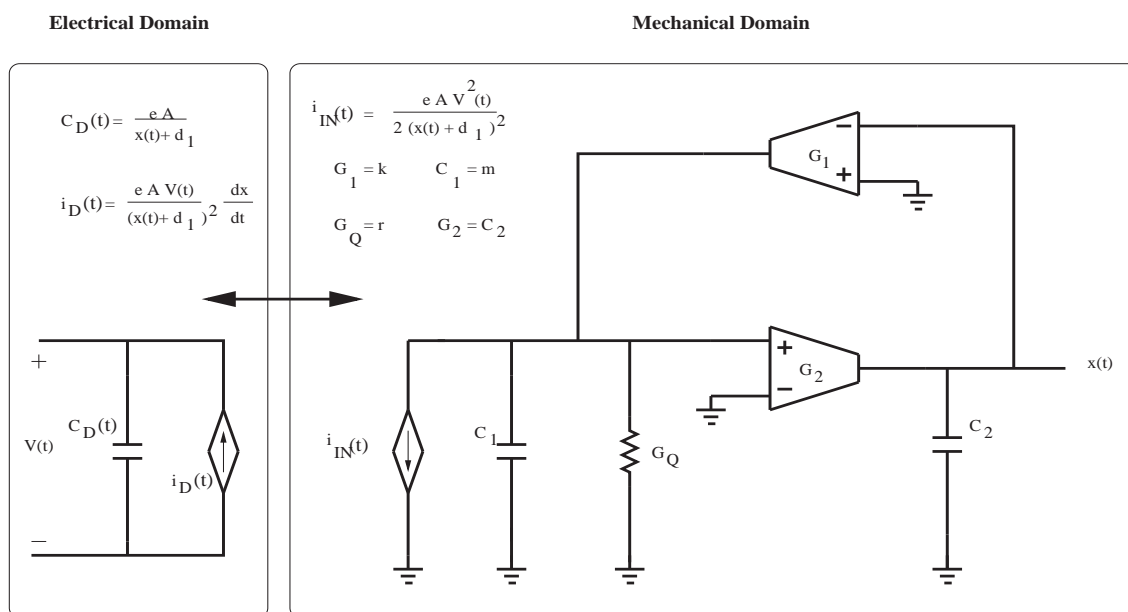


FIGURE 2.6. Equivalent circuit model.

The corresponding equivalent circuit model that was implemented in HSPICE for simulation is shown in Figure 2.7. The transconductors  $G_1$  and  $G_2$  are implemented as voltage dependent current sources. Due to the presence of nonlinear capacitances and current sources, this circuit model cannot be used as such for Spectre simulations.

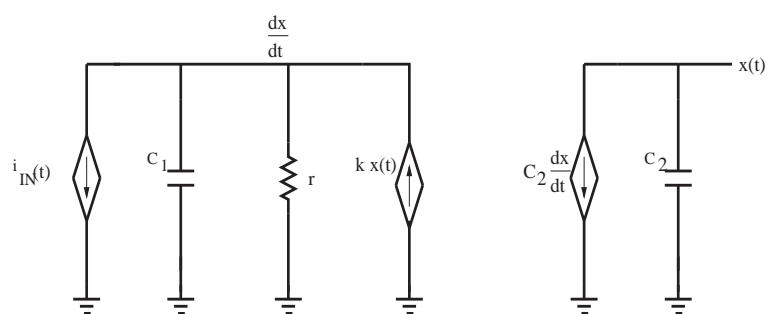


FIGURE 2.7. Equivalent circuit model in HSPICE.

### 2.3.2. Behavioral model

A behavioral model has been developed for use in Spectre simulations. The behavioral model consists of two blocks. The first block captures the mechanical characteristics of the MEMS capacitor using (2.4). The output of the first block is the displacement  $x(t)$ . Based on this output the second block describes the current through the capacitor. The current is computed using (2.10). Figure 2.8 illustrates the model that is implemented using SpectreHDL.

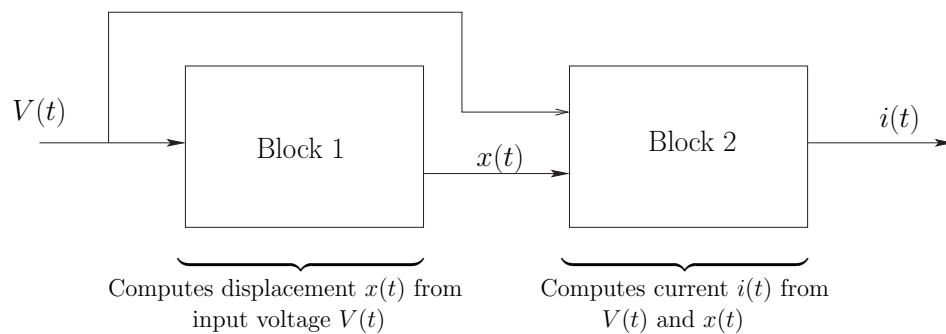


FIGURE 2.8. Behavioral model.

## 2.4. Electrostatic/Numerical Solver

EM8.9 is a simulator for electrostatic MEMS analysis and can accurately simulate the characteristics of MEMS varactors. EM 8.9 employs the finite cloud method (FCM) for mechanical analysis and the boundary cloud method (BCM) for electrostatic analysis. FCM and BCM methods obviate the need for complicated and time consuming mesh generation [10]. Lagrangian descriptions are used to map the electrostatic analysis to the undeformed geometry of conductors, thus eliminating the need for geometry updates and re-computation of the interpolation functions [10]. The procedure for the self-consistent analysis of coupled electromechanical devices can be summarized as follows [10]. Electrostatic

analysis using BCM is done first to compute the surface charge density and the electrostatic pressure, which is then used in the mechanical analysis (performed on the undeformed geometry by FCM) to compute the structural displacement. The geometry is then updated and the capacitance is computed. This procedure is repeated until a state of equilibrium is achieved.

EM8.9 solves for the structural displacement of the MEMS capacitors for a given applied voltage. This solution obtained from EM8.9 is used to compute the capacitance of the MEMS capacitor. The input to EM8.9 is specified in the form of the applied voltage, dimensions, geometry, number of discrete nodes and the material properties. A set of these input parameters defines a unique problem which is processed by EM8.9 in three phases. The first phase is the initialize phase which involves reading in the input, discretization, generating nodes and memory allocation. The second phase is the solve phase where the structural displacement of each discrete element is computed along both the x-axis and the y-axis and stored in the two-dimensional displacement vectors  $xdisp$  and  $ydisp$ . Finally, in the update phase the geometry and displacement vectors are updated. The solve and update phases are repeated until convergence.

The capacitance is computed after the solve phase upon convergence. Since the displacement along the x-axis is small and assuming a sufficiently large number of nodes, each discrete element can be treated as a parallel-plate capacitor, the incremental capacitance between each element and the bottom plate can be computed [6]. Finally, the total capacitance of the MEMS capacitor can be computed by adding all the incremental capacitances.

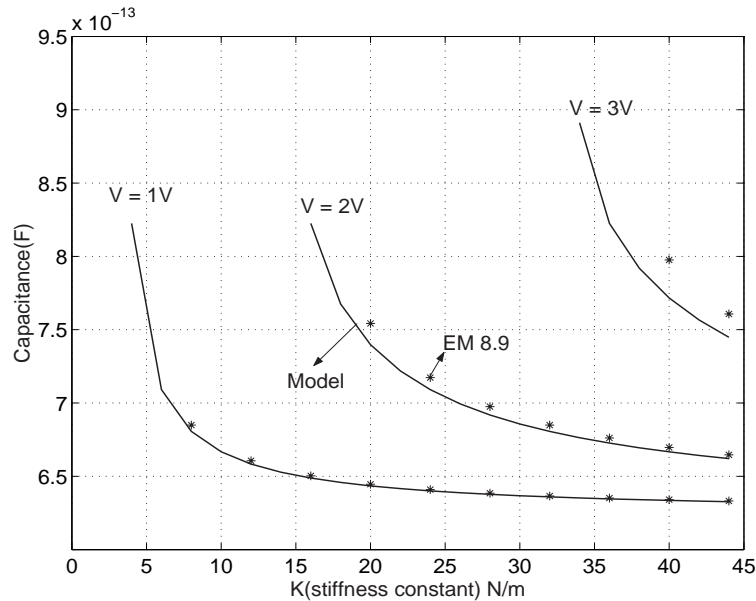


FIGURE 2.9. Capacitance as a function of the stiffness constant.

## 2.5. Results

Simulations were performed for the parallel plate capacitor, cantilever beam capacitor and the fixed-fixed beam capacitor using the high-level models and the numerical solver EM8.9. Different MEMS capacitor structures were simulated using the high-level models and the simulator EM8.9 and their tuning characteristics were compared. An overlap area of  $230 \mu\text{m} \times 230 \mu\text{m}$  and an air gap of  $0.75 \mu\text{m}$  were used for all the structures which results in a nominal capacitance of  $0.624 \text{ pF}$ . As mentioned earlier the stiffness constant of the MEMS varactor is an important design parameter since it determines the tuning ratio of the varactor. Figure 2.9 shows the capacitance as a function of the stiffness constant for different applied voltages. For the parallel plate capacitor the tuning ratio is determined by the stiffness constant of the suspension structure given by (2.9) assuming the capacitor plate is rigid [8]. However, the non-rigid nature

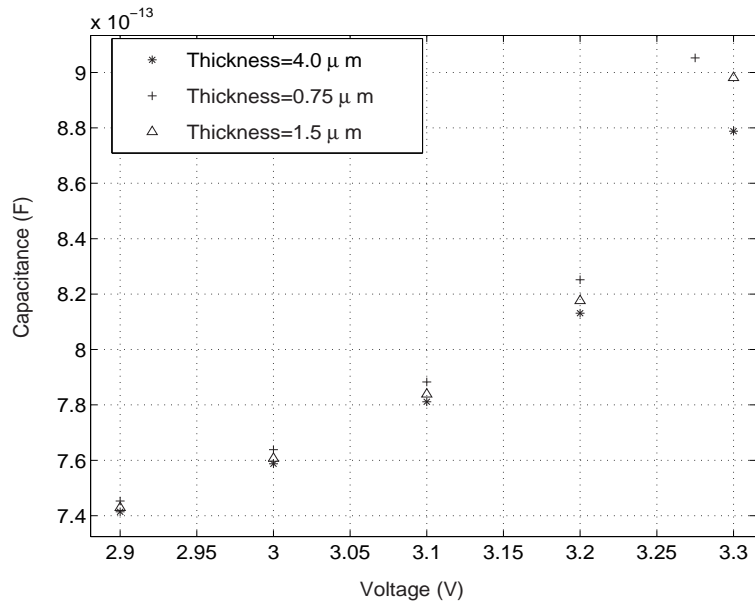


FIGURE 2.10. C-V curves for different thicknesses.

of the suspended plate also contributes to the overall stiffness constant of the MEMS structure. The stiffness constant of the suspended plate depends on its dimensions. Since the length and width (area) of the suspended plate is fixed by the desired capacitance, simulations were done for different thicknesses of the suspended plate. Figure 2.10 shows the capacitance as a function of voltage for different thicknesses of the parallel plate capacitor as simulated by EM8.9. It can be observed that the capacitance tuning characteristic is affected with varying thickness. The increase in the tuning voltage with increasing thickness can be accounted for by the fact that the stiffness constant of the top plate and hence the overall stiffness constant increases with thickness. The high-level models fail to account for the thickness of the top plate and therefore its stiffness constant. This reflects as a discrepancy between the C-V curves obtained from the model and the EM8.9 simulator as shown in Figure 2.11. Simulations performed by using the high-level models show a capacitance tuning ratio of 1.45 for a tuning

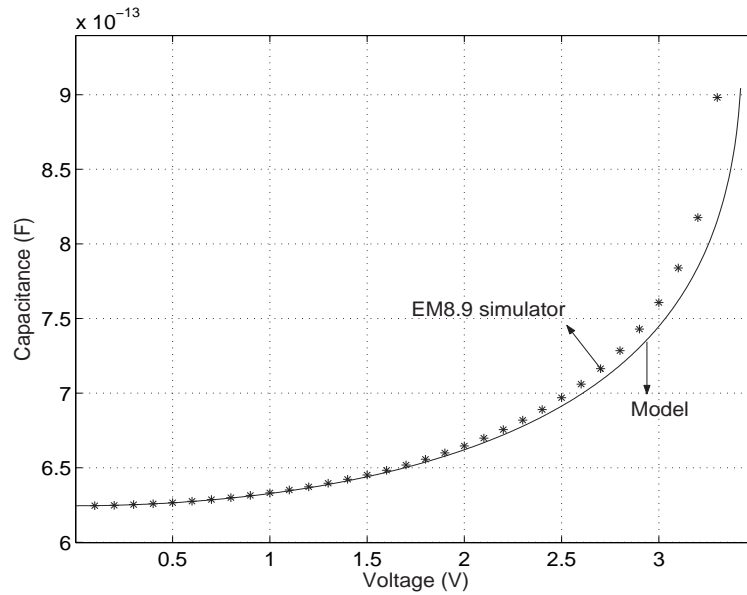
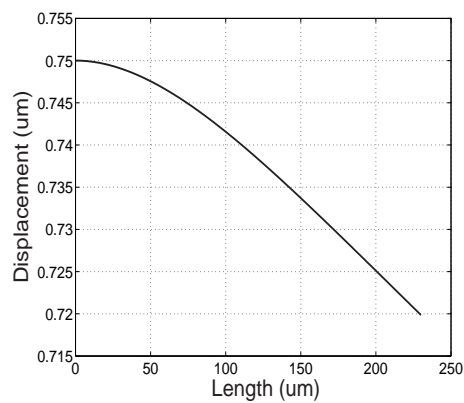


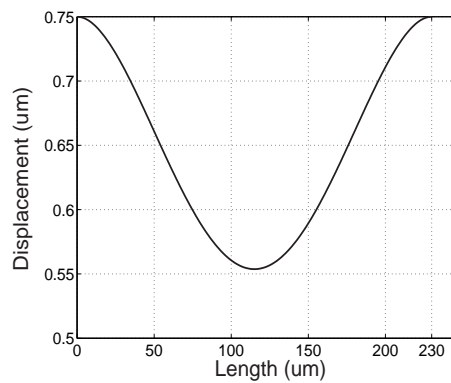
FIGURE 2.11. C-V curve for parallel plate capacitor.

voltage of  $3.42V$ , whereas, the simulated results from EM8.9 show a capacitance tuning ratio of 1.43 for a tuning voltage of  $3.3V$  with an error of 3.6%.

Another drawback of the high-level models is that they are incapable of simulating MEMS capacitor structures such as the cantilever and fixed-fixed beam capacitors. In the parallel plate capacitor with suspension structures the displacement caused by the electrostatic force is uniform along the length of the suspended plate. For the fixed-fixed beam and the cantilever beam capacitors, the displacement of the top plate varies along its length, being maximum at the center for the fixed-fixed beam and at the free end for the cantilever beam. Simulated results obtained from EM8.9 show the structural displacement along the length of the suspended plate in Figures 2.12(a) and (b). Since the high-level models do not account for the change in displacement along the length of the suspended plate, the C-V curves of the cantilever and fixed-fixed beam capacitors as illustrated in Figures 2.13(a) and (b), respectively, deviate significantly from EM8.9.

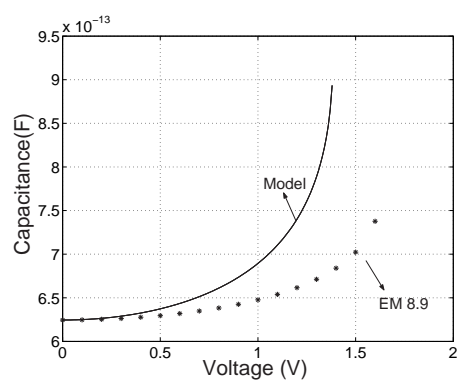


(a)

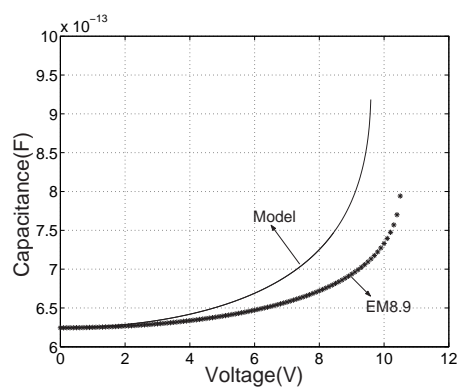


(b)

FIGURE 2.12. Displacement of (a) cantilever beam and (b) fixed-fixed beam.



(a)



(b)

FIGURE 2.13. C-V curve of (a) cantilever beam and (b) fixed-fixed beam.

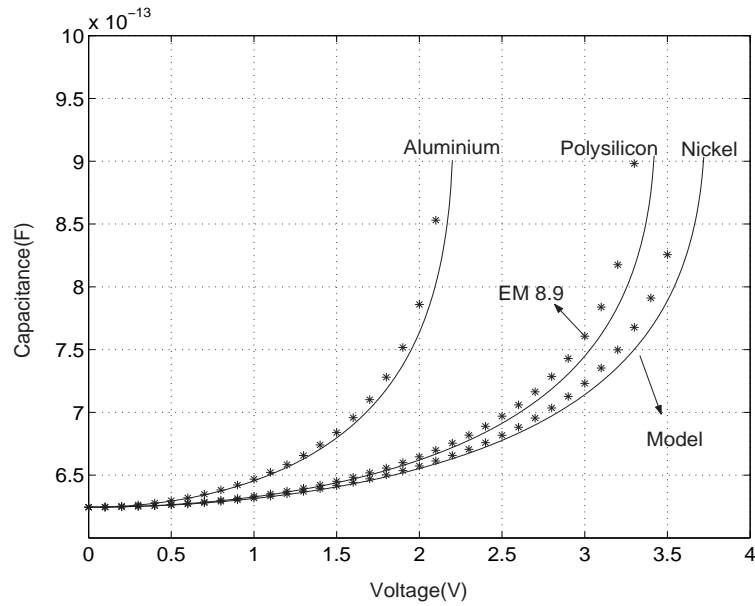


FIGURE 2.14. C-V curve for different materials.

The parallel plate MEMS capacitor structure was simulated for three different materials, polysilicon/gold, aluminum, and nickel/gold. The tuning characteristics obtained from the model and EM8.9 show similar trends as shown in Figure 2.14. However, an error exists between the C-V curves due to reasons discussed earlier.

### 2.5.1. VCO simulations

A 1.6 GHz VCO implemented in a TSMC  $0.35\mu\text{m}$  CMOS technology was simulated. The schematic of the VCO circuit is shown in Figure 2.15. The circuit was simulated using the AHDL model in SpectreS and the coupled circuit/device simulator (SPICE3f5/EM8.9) [12]. The frequency tuning characteristics of this VCO are shown in Figure 2.16. The VCO simulated with the AHDL model shows a tuning range of 1590 MHz to 1640 MHz with a tuning voltage of 2.7 V,

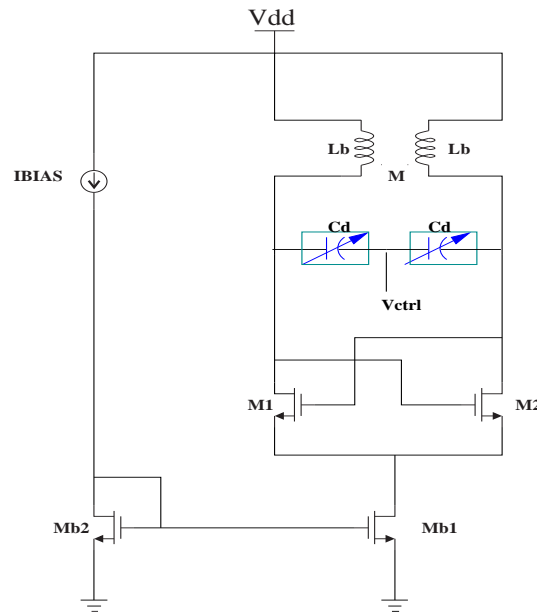


FIGURE 2.15. Voltage controlled oscillator.

whereas, coupled simulations show a tuning range of 1580 MHz to 1640 MHz with the same tuning voltage. The amplitude of oscillation was 2.5 V. The differences in the curves are consistent with differences observed in the corresponding C-V curves. It was also observed that both the AHDL model and the coupled simulator resulted in the same amplitude of oscillation.

## 2.6. Summary

Comparisons between high-level models and a numerical device solver have been presented for the simulation of MEMS based varactors. Issues related to the accuracy of the high-level models have been identified. The high-level models do not account for the stiffness constant of the non-rigid suspended plate and, therefore, an error exists in the C-V curves for higher control voltages. Simulations performed for three different materials also show similar trends. For lower volt-

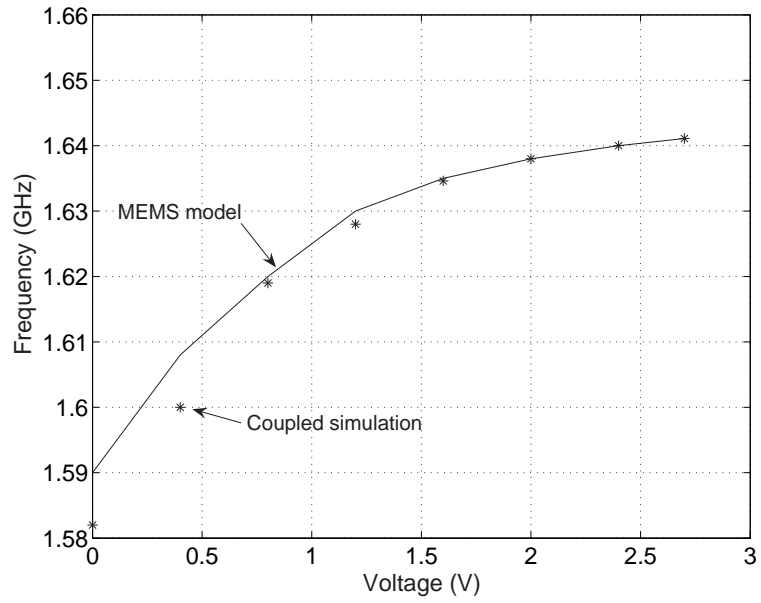


FIGURE 2.16. VCO tuning characteristics.

ages, the high-level models are accurate and can be used for the simulation of RF MEMS VCOs.

### 3. PERIODIC STEADY-STATE ANALYSIS OF RF MEMS VCOs

In general, coupled simulations are very accurate but time consuming. Efficient coupling of the circuit and device simulators is required in order to reduce the run time. The computational time bottleneck is the device simulator which uses numerical models to simulate the device behavior. An improvement in performance can be achieved by reducing the number of device calls. This section examines issues with the simulation of RF MEMS VCOs and suggests a new efficient simulation methodology to simulate these VCOs.

#### 3.1. VCO Simulation Methods

In VCOs, two important specifications of interest to a designer are the frequency tuning range and the phase noise performance. Both these design specifications are determined in the periodic steady state of the oscillator. The steady state can be simulated using the following two approaches,

- (i) Transient analysis
- (ii) Periodic steady-state analysis

##### 3.1.1. Transient analysis

A transient analysis computes the response of a circuit as a function of time. The time interval is decomposed into small individual time intervals and the circuit is solved for each time interval. The two important parameters for a transient analysis are the simulation time and the time steps used during the simulation. In general, these are determined by the following criteria.

- (i) The simulation interval is determined by the largest time constant or the lowest frequency simulated.
- (ii) The time steps that must be used are limited by the highest frequency that a circuit processes.

If the circuit possesses a wide range of time constants, the simulation has to be carried out for a long time with small time steps [13]. To overcome this difficulty, periodic steady-state methods are used. These methods unlike transient analysis only solve periodic steady-state problems.

### 3.1.2. Periodic steady-state analysis

Circuits with a periodic steady-state solution can be simulated using periodic steady-state methods. There are time-domain and frequency-domain methods for computing the periodic steady state. The following paragraph gives a brief overview of the time-domain method.

In the time domain, the underlying differential equations for the circuit are solved by forcing the constraint that the solution is periodic in the steady state. This condition is expressed as  $x(0) = x(T)$ , where  $x$  is the vector of node voltages and  $T$  is the period [14]. In shooting methods, first the circuit is simulated for one period using some guess for the initial condition. Then the final value  $x(T)$  is checked with the guess for the initial value  $x(0)$ . If  $x(0)$  and  $x(T)$  are not the same, the initial value is adjusted. The circuit is simulated again for one period with the adjusted initial value. This process is repeated until the initial value and the final value are in close agreement. Usually the shooting method uses the transient analysis over one period to obtain the final value at the end of the period. The shooting method can be viewed as a transient simulation that is

accelerated for the circuit to approach the periodic steady-state. The acceleration is obtained by adjusting the initial conditions at the beginning of each one-period transient simulation.

The periodic steady-state methods are faster compared with the conventional transient analysis. This work proposes a new simulation methodology using the time-domain shooting method for the simulation of MEMS VCOs.

### 3.2. Simulation Method for RF MEMS VCOs

A MEMS device in a RF VCO will experience high frequency oscillation. Here high frequencies refer to frequencies of oscillation several orders of magnitude larger than the mechanical resonance frequency. The proposed method is applicable only under this condition. Before looking into this approach, it is important to look into the behavior of MEMS capacitors at high frequencies.

#### 3.2.1. Dynamics

In Section 2.2.2 it was shown that MEMS actuators do not respond to frequencies higher than the mechanical resonance frequency. It can be concluded that in a RF VCO, the tank voltage swing does not modulate the value of the displacement and hence the capacitance value. However, consider a MEMS varactor that has a sinusoidal voltage given by  $V_A \sin \omega t$ . The electrostatic force is given by

$$F_e = \frac{-0.5\epsilon_d A (V_A \sin \omega t)^2}{(d_1 + x(t))^2} \quad (3.1)$$

Using trigonometric relations and rearranging the equation,

$$F_e = \frac{-0.5\epsilon_d A}{(d_1 + x(t))^2} V_A^2 (0.5 - 0.5 \cos 2\omega t) \quad (3.2)$$

The above relation shows that the RF voltage gives a DC term, which is equal to the mean square value of the signal voltage, and a second harmonic term. The second harmonic term does not influence the mechanical behavior of the actuator. However, the DC term does affect the displacement of the MEMS actuator and changes the capacitance value.

Simulations show that the response of a MEMS parallel plate actuator to a high frequency sinusoidal excitation is identical to a step response with a step value that is the same as the RMS value of the sinusoidal excitation. A sinusoidal excitation whose frequency is 1 GHz was used for the simulation. The mechanical resonant frequency of the MEMS capacitor is around 30 KHz. Figure 3.1 illustrates the response of a MEMS capacitor to both sinusoidal and step inputs. Hence, the resultant displacement in response to a high frequency signal corresponds to the displacement obtained with the RMS value of the signal. It should be noted that the settling time of the MEMS devices is in the order of tens of microseconds.

### 3.2.2. Simulation approach

In the previous section it has been shown that for a high frequency oscillation the MEMS capacitance value depends on the RMS voltage. If this RMS voltage is known, a single static simulation would be sufficient to compute the MEMS capacitance and hence the steady-state of the oscillator. This idea is used in the proposed simulation approach. Figure 3.2 shows the simulation methodology.

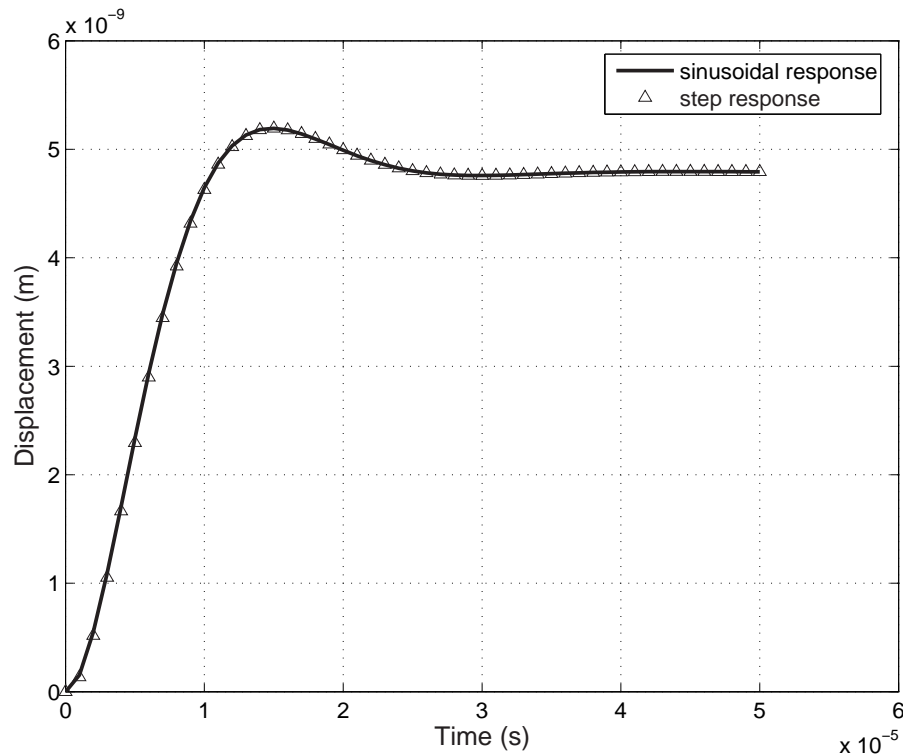


FIGURE 3.1. Comparison between step and sinusoidal responses for a MEMS varactor.

Initially, a DC analysis is used to compute all the node voltages. The DC voltages corresponding to the MEMS capacitors are passed on to the device simulator and the capacitance value is obtained. Based on this capacitance value, a periodic steady-state analysis (PSS) is run using the time-domain shooting method. If the steady-state is achieved, the RMS voltage across the MEMS capacitor is computed. Two parameters, namely  $RMS_{prev}$  and  $RMS_{present}$  are defined for all MEMS capacitor instances. As the name indicates they store the previous and current values of the RMS voltages.  $RMS_{prev}$  and  $RMS_{present}$  are compared to see if their difference is below a certain given value. If this difference exceeds the prescribed value then another PSS iteration is performed to compute

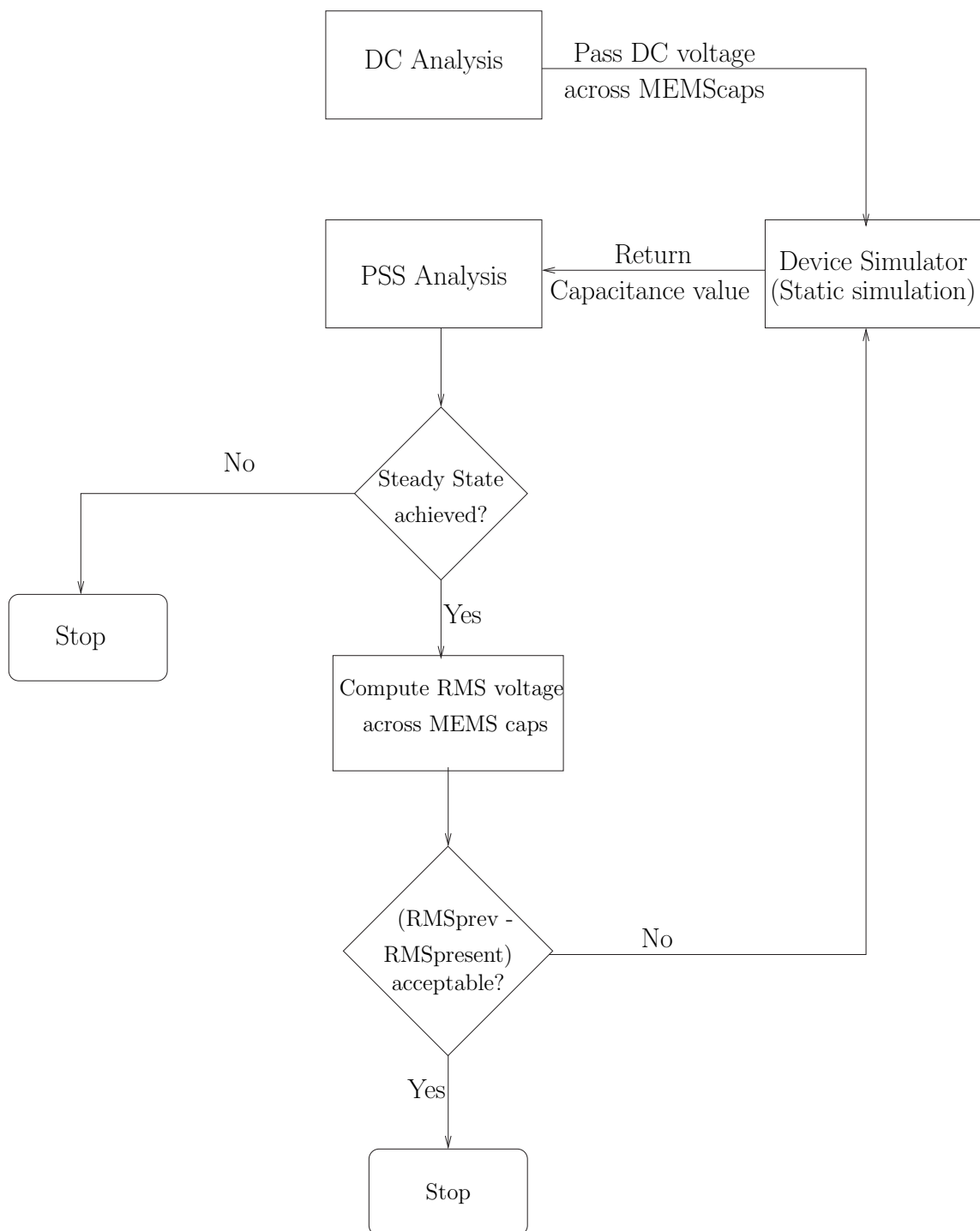


FIGURE 3.2. Flowchart of simulation method.

the steady-state. The PSS analysis is performed iteratively until  $RMS_{prev}$  and  $RMS_{present}$  are close enough.

In this simulation approach at least two PSS iterations are required for convergence. Initially both the parameters ( $RMS_{prev}$  and  $RMS_{present}$ ) are set to zero. At the end of the first PSS iteration,  $RMS_{present}$  takes the current RMS voltage while  $RMS_{prev}$  still retains the initial zero value. At the end of the next PSS iteration  $RMS_{prev}$  is assigned the value from the previous iteration and  $RMS_{present}$  is updated to the new value. Convergence is achieved when the difference between  $RMS_{present}$  and  $RMS_{prev}$  is small.

### 3.3. Simulation of VCOs in COSMO

In COSMO, there are two different methods for computing the steady-state of oscillators. Both these methods use a transient analysis for the VCO simulation but differ in the way in which the MEMS varactor capacitance is computed using the device simulator. One of the method uses static simulations for computing the MEMS device capacitance, while the other method uses a dynamic simulation. A static simulation solves (2.1) for the capacitance computation, while a dynamic simulation solves (2.6). This is the basic difference between the static and dynamic simulation. In this section, we give a brief overview of the simulation methodology in COSMO [6].

#### 3.3.1. Static simulation method

SPICE3f5 and EM8.9 are integrated for static simulations by using file processing and system calls. SPICE3 treats the MEMS capacitor device as a numerical model. At every Newton iteration, SPICE3 computes the node voltages

required by EM8.9 for numerical model evaluation. Then SPICE3 calls EM8.9 using the system command and passes the bias voltages and dimensions of the MEMS capacitor through data files. In response to the call, EM8.9 computes the capacitance by using a static simulation and returns the capacitance value to SPICE3 through another data file. After retrieving the necessary data, SPICE3 loads the capacitance value and updates the circuit matrix and solves the circuit equations.

The MEMS variable capacitor is typically incorporated in a VCO circuit and hence the voltage across it is periodic in time. This method assumes that the device reaches its equilibrium deformed state instantaneously for an applied voltage and the inertial terms in the mechanical equations are neglected. The periodic nature of the voltage across the MEMS capacitor is exploited in reducing the number of device calls. With every device call, the voltage across the MEMS capacitor and the capacitance value obtained from the device is stored in a two dimensional vector *mcap* in increasing order. If the voltage across the MEMS capacitor during any other time step is close to a value stored in *mcap* by a predefined value *VCAPTOL*, the corresponding stored capacitance value is loaded and the numerical computation associated with a device evaluation is skipped. The table is searched using the bisection method so that the appropriate capacitance value is found in approximately  $\log_2 n$  iterations, where  $n$  is the number of points in the table.

### 3.3.2. Dynamic simulation method

In the case of dynamic simulations, the displacement of the MEMS capacitor depends on the past displacement values in addition to the applied voltage

[6]. EM8.9 is embedded in SPICE3 in the form of a subroutine for dynamic simulations. This closed form of coupling is used in COSMO for dynamic simulations. Considering that the device and circuit time constants are widely separated, this method does not call the device simulator for every circuit time step. Rather, the device simulator is called for every hundred or so circuit time steps and, hence, reduces the number of device calls.

### 3.4. Simulation Results

#### 3.4.1. Comparison with transient simulation methods

The simulation approach proposed in this work is much faster compared to the static and dynamic simulation methods discussed in the previous section. A 1.6 GHz LC VCO with two MEMS devices acting as variable capacitors shown in Figure 2.15 takes approximately 4 weeks for a simulation interval of  $60\mu s$  using a dynamic simulation method. A static simulation method requires approximately 3-4 days of simulation time, while the proposed simulation approach takes about 20 minutes. The new method required just four static simulation runs or device calls. In [6], an estimation of the number of device calls required by the static and dynamic simulation methods is given. Consider a 1 GHz VCO with a MEMS device that takes  $20\mu s$  to settle. Assuming that 100 time points per cycle are needed for an accurate transient simulation,  $20,000 \times 100$  device calls need to be made. Although in the static simulation method there is a considerable reduction in the number of device calls compared to a dynamic simulation, it is still high. Simulation results in [6] indicate the number of device calls to be of the order of a thousand. The proposed method significantly reduces the number of device calls and hence improves the simulation time significantly.

### 3.4.2. VCO simulations

A 1.6 GHz VCO as shown in Figure 2.15 was simulated to obtain the tuning characteristics using the proposed method. Simulations were carried out using a relative tolerance of  $10^{-6}$ . A comparison with the results obtained from static simulations shows good agreement as shown in Figure 3.3. The proposed method deviates from the static simulation method by a maximum of 0.25%.

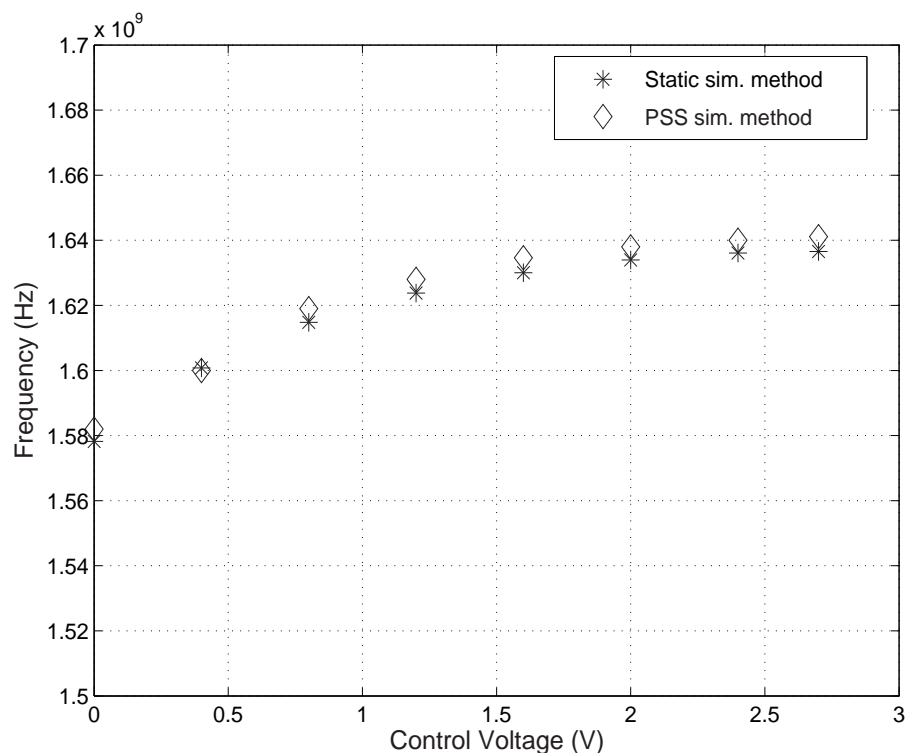


FIGURE 3.3. VCO tuning characteristics from the static simulation and periodic steady-state methods.

### 3.5. Summary

In this chapter, we observed that MEMS based RF VCOs have a wide range of time constants. Computation of the oscillator steady-state using tran-

sient simulations requires an excessive number of device calls. A reduction in the number of device calls is necessary to improve the speed of coupled simulations. Based on the dynamic behavior of MEMS based varactors, a simulation methodology using the time-domain shooting method has been proposed. Comparisons with transient simulation methods show that there is a significant reduction in the number of device calls.

## 4. PHASE NOISE IN MEMS VCOs

In order to simulate and characterize the effect of noise on the performance of an electronic circuit or system, it is important to investigate the noise sources in the system and develop models for these noise sources [15]. This chapter presents an overview of the mechanical noise exhibited by MEMS variable capacitors and its effect on the VCO phase noise. A simple model is developed to characterize this mechanical noise as a current source in the electrical domain. An accurate phase noise analysis technique is used to simulate the noise contribution from MEMS variable capacitors.

### 4.1. Overview

#### 4.1.1. Mechanical noise

Electrostatic actuators exhibit noise due to random mechanical vibrations. Molecules from the surrounding gas collide with the suspended plate and generate a noise force known as Brownian noise. The fluctuating noise force has a white spectral density given by [3]

$$F_N = \sqrt{4k_B T r} \quad (4.1)$$

where  $k_B$  is the Boltzmann's constant,  $T$  is the absolute temperature and  $r$  is the damping coefficient. This noise force is responsible for the noisy vibrations of the suspended plate.

### 4.1.2. Displacement noise power spectral density

Consider the following equation describing the dynamics of an electrostatic actuator

$$m \frac{d^2x}{dt^2} + r \frac{dx}{dt} + kx = F_e \quad (4.2)$$

where  $F_e$  is the input driving force. The transfer function between the displacement  $X(s)$  and the input force  $F_e(s)$  can be obtained from (4.2) using Laplace transforms and is given as follows,

$$\frac{X(s)}{F_e(s)} = \frac{1/m}{s^2 + \frac{\omega_n}{Q_M} s + \frac{k}{m}} \quad (4.3)$$

where the mechanical resonant frequency  $\omega_n = \sqrt{\frac{k}{m}}$  and  $Q_M = \frac{\omega_n m}{r}$ .

The white power spectral density of the noise force  $F_N$  is shaped by the low pass characteristics of the above transfer function. The displacement noise power spectral density can be computed from the above transfer function as follows [3],

$$\overline{X_n^2(\omega)} = F_N^2 \left| \frac{X(s)}{F_e(s)} \Big|_{s=j\omega} \right|^2 \quad (4.4)$$

Substituting (4.1) and (4.3) in the above equation we obtain,

$$\overline{X_n^2(\omega)} = \frac{4k_B T r}{k^2 \left[ \left(1 - \frac{\omega^2}{\omega_n^2}\right)^2 + \frac{1}{Q_M^2} \frac{\omega^2}{\omega_n^2} \right]} \quad (4.5)$$

The noise power spectral density on a log scale is shown in Figure 4.1. For frequencies higher than the resonant frequency, the noise power spectral density rolls off at -40 dB/dec. Further it shows peaking at the mechanical resonant frequency  $\omega_n$ . Increasing  $Q_m$  concentrates the noise at  $\omega_n$  and reduces it elsewhere.

The electrostatic actuator is used as a variable capacitor in a VCO tank. It is important to see how the Brownian noise transforms into phase noise in the VCO.

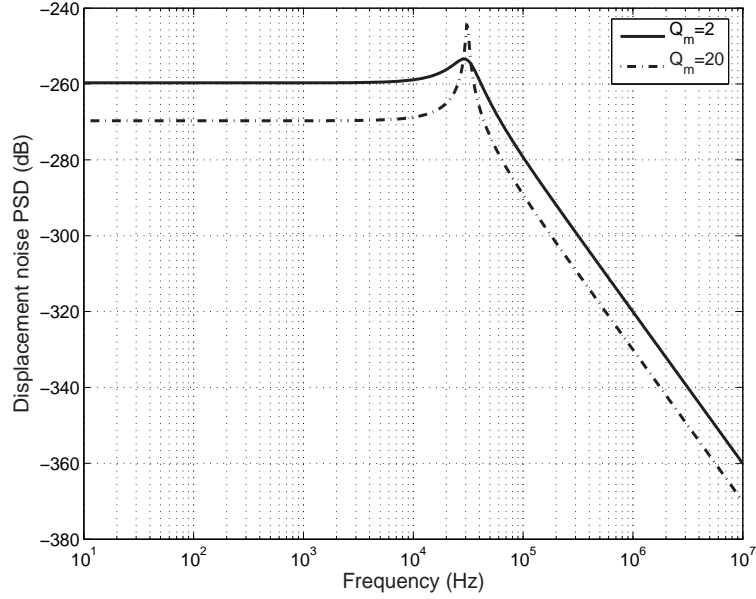


FIGURE 4.1. Displacement noise power spectral density.

#### 4.2. Brownian Motion Induced Phase Noise

The random mechanical-thermal vibration from the variable capacitors induces additional phase noise in a MEMS VCO. The vibration of the suspended plates in an electrostatic actuator causes variation in the capacitance value which causes frequency modulation at the VCO output. The resulting FM sidebands around the oscillation frequency appear as phase noise which is given by [3]

$$S_{\theta}(f_m)_{Mechanical} = \frac{\overline{X_n^2(f_m)}}{8 \left(\frac{1+\alpha}{\alpha}\right)^2 N x_o^2} \left(\frac{f_o}{f_m}\right)^2 \quad (4.6)$$

where  $X_n^2(f_m)$  is the displacement noise power spectral density of the suspended plate described by (4.5),  $x_o$  is the nominal air gap of the variable capacitor,  $N$  is the number of parallel micromachined capacitors,  $\alpha$  is the ratio of the nominal tank tunable capacitance and its parasitics,  $f_o$  and  $f_m$  are the oscillation frequency and the offset frequency of interest, respectively.

Figure 4.1 shows that the displacement noise power spectral density of the micromachined capacitor is constant below the mechanical resonant frequency,  $\omega_n$ , and decays at 40 dB per decade above  $\omega_n$ . Hence, the resulting phase noise profile in (4.6) shows a 20 dB and 60 dB per decade fall before and after the offset frequency  $\omega_n$ , respectively. The phase noise at  $\omega_n$  shows peaking for different values of  $Q_m$ . Figure 4.2 shows a typical Brownian motion induced phase noise plot.

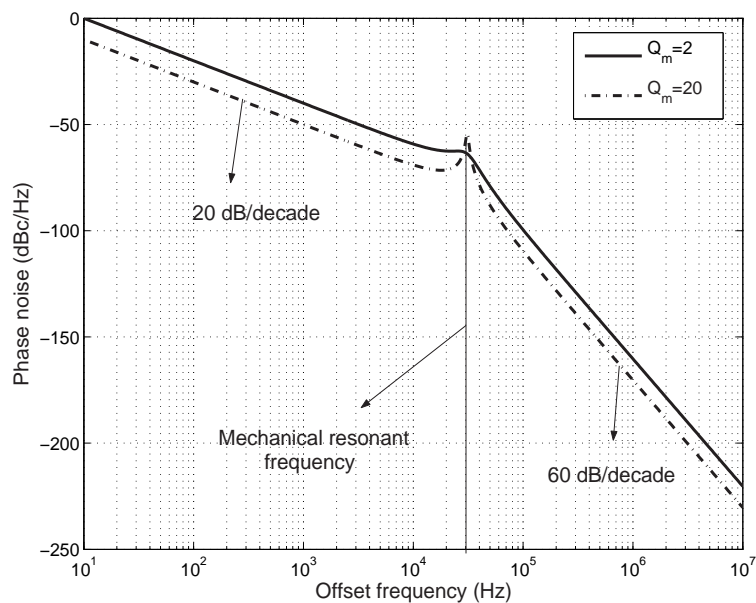


FIGURE 4.2. Brownian motion induced phase noise.

### 4.3. Noise Current Modeling

Equation (4.6) gives a good estimate of the phase noise due to the MEMS variable capacitors. It shows how capacitor design parameters affect the VCO phase noise and provides a design insight. However, (4.6) is not useful for simulation purposes for the the following reasons:

- The term  $\alpha$  in (4.6), which is the ratio of the tunable capacitance and the parasitics in the tank, cannot be defined accurately. This is because the parasitics also include the nonlinear device capacitances which vary with the large-signal steady state.
- Existing phase noise simulation methods require device noise to be modeled as a current or voltage source.

This work has modeled Brownian noise as a current source in parallel with the MEMS variable capacitor. We start out with a voltage-current equation for a MEMS variable capacitor and derive the current noise power spectral density based on the noise models provided in [15].

The voltage current relationship in a MEMS variable capacitor is given by [8]

$$i(t) = C(t) \frac{dV(t)}{dt} + V(t) \frac{dC(t)}{dt} \quad (4.7)$$

where  $C(t)$  is given by

$$C(t) = \frac{\varepsilon_o A}{x_o + x_{sig}(t) + x_n(t)} \quad (4.8)$$

where  $\varepsilon_o$  is the dielectric permittivity of air,  $A$  is the area of the MEMS capacitor plates,  $x_o$  is the nominal air gap of the variable capacitor,  $x_{sig}$  is the steady-state value of the displacement in response to an input signal  $V(t)$ , and  $x_n(t)$  is the noisy displacement of the suspended plate caused by the Brownian motion of gas molecules.

The MEMS variable capacitor experiences high frequency signals across its terminals in a VCO. Section 3.2.1 shows that the swing of the VCO tank does not modulate the displacement of the MEMS variable capacitor. Furthermore the

steady-state displacement of the MEMS varactor in response to a high frequency sinusoid is a constant function of time that depends on the RMS value of the signal. Hence  $x_{sig}(t)$  in (4.8) is a constant, whose magnitude depends on the RMS value of the signal.

Based on the above observation, let  $x_{ss} = x_o + x_{sig}$ . Rewriting the expression for  $C(t)$

$$C(t) = \frac{\epsilon_o A}{x_{ss} + x_n(t)} \quad (4.9)$$

We further assume that the noisy displacement given by  $x_n(t)$  is small compared to  $x_{ss}$  and (4.9) can be written as a series expansion given by

$$C(t) = \frac{\epsilon_o A}{x_{ss} \left(1 + \frac{x_n(t)}{x_{ss}}\right)} \cong \frac{\epsilon_o A}{x_{ss}} \left(1 - \frac{x_n(t)}{x_{ss}}\right) \quad (4.10)$$

Substituting (4.10) in (4.7) and rearranging, one obtains

$$i(t) = \underbrace{\frac{\epsilon_o A}{x_{ss}} \frac{dV(t)}{dt}}_{i_c(t)} - \underbrace{\frac{\epsilon_o A}{x_{ss}^2} x_n(t) \frac{dV(t)}{dt}}_{\text{noise current}(i_{n1}(t))} - \underbrace{\frac{\epsilon_o A}{x_{ss}^2} V(t) \frac{dx_n(t)}{dt}}_{\text{noise current}(i_{n2}(t))} \quad (4.11)$$

Equation (4.11) shows that there are two noise current terms. Figure 4.3 illustrates the noise model for the MEMS capacitor.

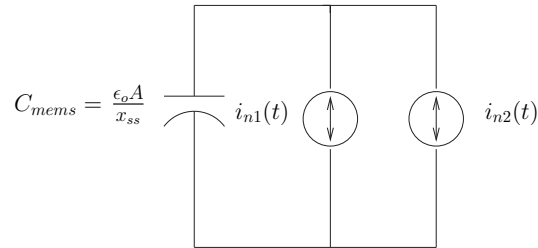


FIGURE 4.3. Noise current model for the MEMS capacitor.

#### 4.4. Current Noise Power Spectral Density

The objective is to derive a current noise power spectral density. The noise current in the time domain is given by (4.11). With that equation as a starting point we arrive at the power spectral density of the two terms and show that the noise contribution of  $i_{n2}(t)$  (term 2) is negligible compared to that of  $i_{n1}(t)$  (term 1).

##### 4.4.1. Noise contribution from term 1

The noisy current is given by

$$i_{n1}(t) = \frac{\varepsilon_o A}{x_{ss}^2} x_n(t) \frac{dV(t)}{dt} \quad (4.12)$$

(4.12) shows how the noisy displacement transforms into a noise current. In order to understand the process by which Brownian noise transforms into noise current, a noise model is derived. Using this model, the noise power spectral density is derived.

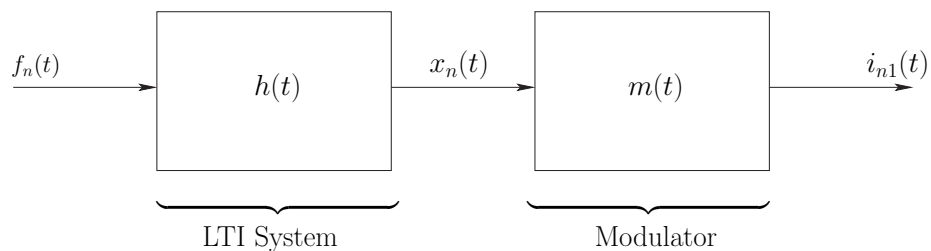


FIGURE 4.4. Noise model describing the conversion of Brownian noise into a noise current.

The noise model shown in Figure 4.4 consists of two blocks. Section 4.1 shows that the electrostatic actuator can be identified as a LTI system with a low pass transfer function given by (4.3). The first block captures this low pass characteristics of the electrostatic actuator. The Brownian noise that gives rise to

a noisy displacement with power spectral density given by (4.5) is shaped by this filter. The input to this block is the Brownian noise with power spectral density given by (4.1).

The second block is modeled as a modulator whose output is given by (4.13).

$$i_{n1}(t) = x_n(t)m(t) \quad (4.13)$$

This block captures the time domain multiplication in (4.13). Comparing (4.12) and (4.13), the modulating function  $m(t)$  is given by

$$m(t) = \frac{\varepsilon_o A}{x_{ss}^2} \frac{dV(t)}{dt} \quad (4.14)$$

The noise model decouples the noise process into mechanical and electrical domains. The first block transforms the Brownian noise, which is a mechanical force, into noisy displacements. The second block converts the mechanical vibrations into electrical current through a modulation function.

The noise power spectral density is defined as the Fourier transform of the auto-correlation function [16]. Hence, we start out by deriving the auto-correlation function of the noise process described by the above model. In [15] similar types of noise models have been discussed and the noise power spectral density for these is derived. We go through the derivation with some simplification to obtain the power spectral density of the current noise.

Consider the output  $x_n(t)$  of the first block. The power spectral density ( $\overline{X_n^2(\omega)}$ ) is given by (4.5). Since this is a LTI system the auto-correlation function is given by the inverse Fourier transform of  $\overline{X_n^2(\omega)}$ ,

$$R_x(\tau) = \mathcal{F}^{-1}\{\overline{X_n^2(\omega)}\} \quad (4.15)$$

$R_x(\tau)$  represents the auto-correlation function of the stationary process described by the first block.

The second block in the model is a modulator with a modulating function  $m(t)$ . It should be noted that  $m(t)$  is periodic. Considering that the MEMS capacitor is connected across the tank of the VCO, the voltage across its terminal  $V(t)$  is periodic.  $m(t)$  given by (4.14) is a function of  $\frac{dV(t)}{dt}$  and, hence, is periodic. Since  $m(t)$  is periodic the second block is a periodically time varying system. For simplicity assume  $V(t) = V_{amp} \sin \omega_o t$ , then  $m(t)$  is given by

$$m(t) = \frac{\varepsilon_o A}{x_{ss}^2} \omega_o V_{amp} \cos \omega_o t \quad (4.16)$$

The auto-correlation of  $i_{n1}(t)$  is given by

$$R_i(t, \tau) = E\{x_n(t + \tau/2)m(t + \tau/2)x_n(t - \tau/2)m(t - \tau/2)\} \quad (4.17)$$

Since  $m(t)$  is deterministic,  $R_i(t, \tau)$  can be written as

$$R_i(t, \tau) = R_x(\tau)m(t + \tau/2)m(t - \tau/2) \quad (4.18)$$

where  $R_x(\tau)$  is the auto-correlation function of the stationary process described by the first block. Substituting for  $m(t)$  in (4.18)

$$R_i(t, \tau) = R_x(\tau) \left( \frac{\varepsilon_o A}{x_{ss}^2} \omega_o V_{amp} \right)^2 \cos \omega_o(t + \tau/2) \cos \omega_o(t - \tau/2) \quad (4.19)$$

It should be noted that  $R_i(t, \tau)$  is the auto-correlation function for a cyclostationary process. It is periodic in  $t$  and can be expressed as a Fourier series. Hence we can rewrite (4.19) as a complex exponential and obtain the Fourier series coefficients. These Fourier series coefficients are called the harmonic auto-correlation functions [19]. For convenience let us assume  $k = \left( \frac{\varepsilon_o A}{x_{ss}^2} \omega_o V_{amp} \right)^2$ .

$$R_i(t, \tau) = R_x(\tau)k \left( \frac{e^{j\omega_o(t+\tau/2)} + e^{-j\omega_o(t+\tau/2)}}{2} \right) \left( \frac{e^{j\omega_o(t-\tau/2)} + e^{-j\omega_o(t-\tau/2)}}{2} \right) \quad (4.20)$$

Upon simplification,

$$R_i(t, \tau) = \frac{R_x(\tau)k}{4} (e^{j\omega_o\tau} + e^{-j\omega_o\tau} + e^{j2\omega_o t} + e^{-j2\omega_o t}) \quad (4.21)$$

From (4.21) the Fourier series coefficients  $R_i^{(n)}(\tau)$  are given as follows. The superscript  $n$  represents the coefficient of the  $n^{\text{th}}$  harmonic.

$$\left. \begin{aligned} R_i^{(0)}(\tau) &= \frac{R_x(\tau)k}{4} (e^{j\omega_o\tau} + e^{-j\omega_o\tau}) \\ R_i^{(2)}(\tau) &= \frac{R_x(\tau)k}{4} \\ R_i^{(-2)}(\tau) &= \frac{R_x(\tau)k}{4} \end{aligned} \right\} \quad (4.22)$$

A cyclostationary process is characterized by a time varying power spectral density  $S_i^{(n)}(t, \omega)$  that is periodic in  $t$  and can be expressed as a Fourier series [16]. The Fourier series coefficients  $S_i^{(n)}(\omega)$  are given by the Fourier transform of the harmonic auto-correlation functions [19].

$$S_i^{(n)}(\omega) = \mathcal{F}\{R_i^{(n)}(\tau)\} \quad (4.23)$$

The Fourier series coefficients  $S_i^{(n)}(\omega)$  of the time varying spectral density  $S_i^{(n)}(t, \omega)$  are called harmonic power spectral densities (HPSDs) [19]. Applying the Fourier transform to  $R_i^{(n)}(\tau)$ , the HPSDs are given by (4.24). Figure 4.5 shows the HPSDs of the time varying power spectral density. It should be noted that the zeroth Fourier coefficient ( $S_i^{(0)}(\omega)$ ) is the stationary power spectral density of the noise source and it is termed as the time average power spectral density.

$$\left. \begin{aligned} S_i^{(0)}(\omega) &= k \frac{\overline{X_n^2(\omega - \omega_o)}}{4} + k \frac{\overline{X_n^2(\omega + \omega_o)}}{4} \\ S_i^{(2)}(\omega) &= k \frac{\overline{X_n^2(\omega)}}{4} \\ S_i^{(-2)}(\omega) &= k \frac{\overline{X_n^2(\omega)}}{4} \end{aligned} \right\} \quad (4.24)$$

The current noise power spectral density arising from term 1 is cyclostationary and is completely characterized by its HPSDs. [17] points out that the

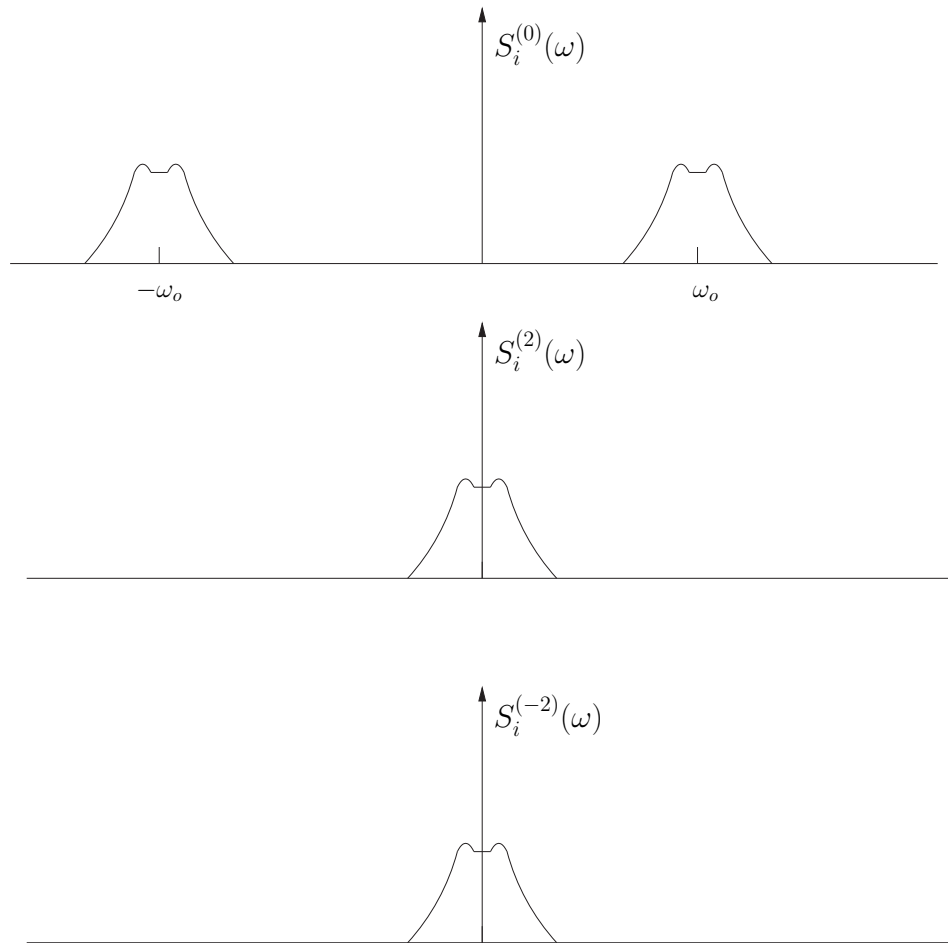


FIGURE 4.5. HPSDs of the time varying power spectral density.

output noise of an oscillator is stationary. Hence we are interested in the time average power spectral density.

The time average power spectral density can be obtained in a more intuitive way. It is worth going through this alternate method. A similar method will be adopted to obtain the noise PSD contribution of the second term. We start out with taking a Fourier transform of (4.12).

$$i_{n1}(\omega) = \frac{\varepsilon_o A}{x_{ss}^2} \mathcal{F} \left\{ x_n(t) \frac{dV(t)}{dt} \right\} \quad (4.25)$$

It should be noted that  $\frac{dV(t)}{dt}$  is periodic and is given by  $\frac{dV(t)}{dt} = V_{amp} \cos \omega_o t$ . Since multiplication in the time domain corresponds to convolution in the frequency domain, the above equation can be rewritten as,

$$i_{n1}(\omega) = \frac{\varepsilon_o A}{x_{ss}^2} \frac{1}{2} \omega_o V_{amp} [X_n(\omega) \otimes (\delta(\omega - \omega_o) + \delta(\omega + \omega_o))] \quad (4.26)$$

where  $\otimes$  represents the convolution operation. The frequency domain convolution modifies the above equation as follows,

$$i_{n1}(\omega) = \frac{\varepsilon_o A}{x_{ss}^2} \omega_o V_{amp} \frac{1}{2} [X_n(\omega - \omega_o) + X_n(\omega + \omega_o)] \quad (4.27)$$

$i_{n1}(\omega)$  represents the current noise spectrum. The current noise PSD is given by,

$$\overline{i_{n1}^2} = i_{n1} i_{n1}^* \quad (4.28)$$

where  $i_{n1}^*$  represents the complex conjugate of  $i_{n1}$ . Based on the above equation, the current noise power spectral density is as follows,

$$\overline{i_{n1}^2(\omega)} = \left( \frac{\varepsilon_o A}{x_{ss}^2} \omega_o V_{amp} \right)^2 \frac{1}{4} [\overline{X_n^2(\omega - \omega_o)} + \overline{X_n^2(\omega + \omega_o)}] \quad (4.29)$$

$\overline{i_{n1}^2(\omega)}$  is the same as  $S_i^{(0)}(\omega)$  and hence represents the time average power spectral density. The time average power spectral density  $\overline{i_{n1}^2(\omega)}$  can be seen as an upconversion of the displacement noise from the baseband to the oscillation frequency. This upconversion is due to the fact that the noisy displacement undergoes a time domain multiplication before it appears as a noisy current.

#### 4.4.2. Noise contribution from term 2

We follow a similar approach to obtain the time average noise power spectral density from term 2. From (4.11)  $i_{n2}(t)$  is given by

$$i_{n2}(t) = \frac{\varepsilon_o A}{x_{ss}^2} V(t) \frac{dx_n(t)}{dt} \quad (4.30)$$

Substituting for  $V(t) = V_{amp} \sin \omega_o t$  and taking the Fourier transform, the current noise spectrum  $i_{n2}(j\omega)$  is given by

$$i_{n2}(\omega) = \frac{\varepsilon_o A}{x_{ss}^2} \frac{1}{2} \omega_o V_{amp} [\omega X_n(\omega) \otimes (\delta(\omega - \omega_o) + \delta(\omega + \omega_o))] \quad (4.31)$$

The time average power spectral density  $i_{n2}^2(\omega)$  is given by

$$\overline{i_{n2}^2(\omega)} = \left( \frac{\varepsilon_o A}{x_{ss}^2} \right)^2 \frac{V_{amp}^2}{4} \left[ |\omega - \omega_o|^2 \overline{X_n^2(\omega - \omega_o)} + |\omega + \omega_o|^2 \overline{X_n^2(\omega + \omega_o)} \right] \quad (4.32)$$

Figure 4.6 shows a comparison of the noise current PSDs of both the terms  $i_{n1}(t)$  and  $i_{n2}(t)$  normalized to the current term  $i_c(t)$  in (4.11). It is clear that the

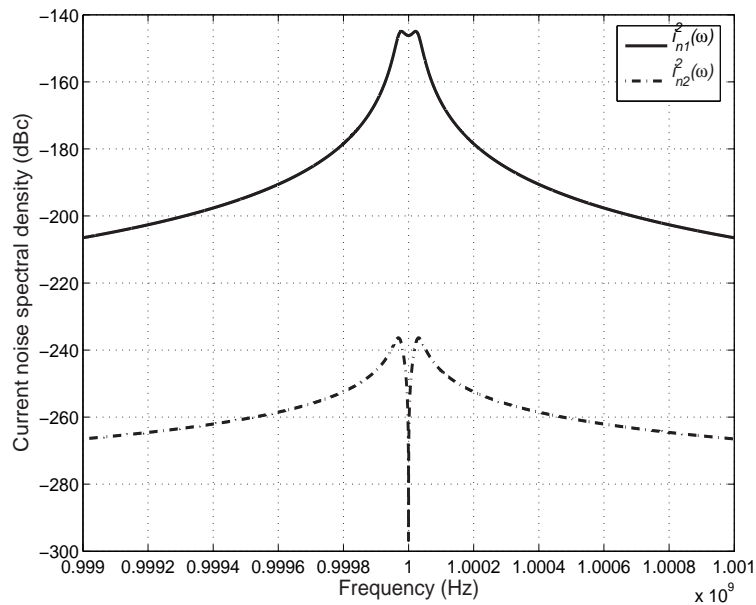


FIGURE 4.6. Normalized current noise power spectral densities.

noise contribution from term 1 is dominant. For phase noise computation we can neglect the effect of the noise arising from term 2.

## 4.5. Phase Noise Calculation Technique

This work uses the nonlinear perturbation technique proposed in [17] and [18] for phase noise computation. We will briefly describe the method and explain how the phase noise contribution from the MEMS capacitors needs to be evaluated using this technique.

### 4.5.1. Nonlinear perturbation analysis

An oscillator perturbed by a noise source experiences phase and orbital deviation. If  $x_s(t)$  is the periodic response of an unperturbed oscillator, the perturbed response is given by  $x_s(t + \alpha(t)) + y(t)$ .  $\alpha(t)$  is a changing time shift or phase deviation and  $y(t)$  is termed as an orbital deviation. Jitter and spectral spreading (Phase noise) are dependent on how  $\alpha(t)$  spreads with time. Generally any perturbed nonlinear system is analyzed by linearizing around the unperturbed solution under the assumption that the resultant deviation is small. [17] shows that the above assumption is not valid for oscillators. In fact, the phase error grows exactly linearly with time [17].

After rigorous derivations [18] shows that the single sideband phase noise spectrum is given by (4.33)

$$\mathcal{L}(\omega_m) = 10 \log_{10} \left( \frac{\omega_o^2 c(\omega_m)}{\pi^2 \omega_o^4 c^2(\omega_m) + \omega_m^2} \right) \quad (4.33)$$

where  $\omega_o$  is the oscillation frequency,  $\omega_m$  is the offset frequency and  $c(\omega_m)$  is a scalar quantity that gives the contribution of all the noise sources to the phase noise spectrum.  $c(\omega_m)$  is given by (4.34)

$$c(\omega_m) = c_w + \sum_{m=1}^M |V_{0m}|^2 S_{Nm}(f) \quad (4.34)$$

where  $c_w$  is the contribution of white noise sources. The second term in (4.34) gives the total contribution of  $M$  colored noise sources.  $S_{Nm}(f)$  is the power spectral density of the  $m^{\text{th}}$  colored noise source.  $c_w$  and  $V_{0m}$  are defined as follows.

$$c_w = \frac{1}{T} \int_0^T v_1^T(\tau) B_w(x_s(\tau)) B_w^T(x_s(\tau)) v_1(\tau) d\tau \quad (4.35)$$

$$V_{0m} = \frac{1}{T} \int_0^T v_1^T(\tau) B_{cm}(x_s(\tau)) d\tau \quad m = 1, \dots, M. \quad (4.36)$$

$v_1(\tau)$  is called the perturbation projection vector (PPV). The PPV is a periodic vector which serves as a transfer function from the noise sources to the scalar  $c$  and hence to the overall phase noise power spectral density [20].  $B_w(x_s(\tau))$  is a state dependent matrix that maps white noise sources with unity PSD to the system of differential algebraic equations (DAEs).  $B_{cm}(x_s(\tau))$  is a state dependent vector that maps the  $m^{\text{th}}$  colored noise source to the system of DAEs. In general,  $B_w$  and  $B_{cm}$  capture the modulation of white and colored noise sources in the large-signal steady-state.

#### 4.5.2. Simulating Brownian motion induced phase noise

The current noise spectral density given by  $\overline{i_{n1}^2(\omega)}$  is a colored noise source. Consider the following equation which gives the contribution of colored noise sources to the scalar quantity  $c$ .

$$c_{cm} = \sum_{m=1}^M |V_{0m}|^2 S_{Nm}(f) \quad m = 1, \dots, M. \quad (4.37)$$

$S_{Nm}(f)$  denotes the colored noise spectral density. It is important to emphasize the fact that the current noise spectral density given by  $\overline{i_{n1}^2(\omega)}$  cannot be directly used in the above equation for phase noise computation.  $\overline{i_{n1}^2(\omega)}$  has a bandpass

characteristic and this phase noise analysis technique cannot handle bandpass noise sources [18].

The process by which Brownian noise transforms into a current noise is cyclostationary. [17] and [18] adopt a modulated stationary noise model for cyclostationary noise generators. The noise model developed in the previous section shows that the  $i_{n1}(t)$  is a result of the modulation of  $x_n(t)$ . The modulation function is given by  $m(t)$  which is a function of the large-signal steady-state of the VCO. For colored noise sources the vector  $B_{cm}$  captures the large signal modulation. Hence  $m(t)$  becomes  $B_{cm}$  in Eq. (4.36) which can be rewritten as follows,

$$V_{0mems} = \frac{1}{T} \int_0^T v_1^T(\tau)m(\tau)d\tau \quad (4.38)$$

The above formulation is used in (4.37) to evaluate the noise contribution of MEMS capacitors.  $S_{Nm}(f)$  in (4.37) will be the same as the displacement noise power spectral density in (4.5). Eq.(4.37) can be formulated as,

$$c_{mems} = \sum_{m=1}^M |V_{0mems}|^2 \overline{X_n^2(f)} \quad (4.39)$$

Hence Eq.(4.39) can be used in (4.34) and subsequently in (4.33) to compute the phase noise contribution of the MEMS capacitors.

#### 4.6. Equivalent Circuit Model for Brownian Noise

In Section 2.3, high-level models to simulate the electro-mechanical behavior of MEMS varactors were discussed. However, these models do not account for the mechanical noise and, hence, they cannot be used to simulate the phase noise performance in RF MEMS VCOs. This section develops an equivalent circuit to model the Brownian noise in MEMS varactors. Consider a simple RLC series circuit as shown in Figure 4.7.

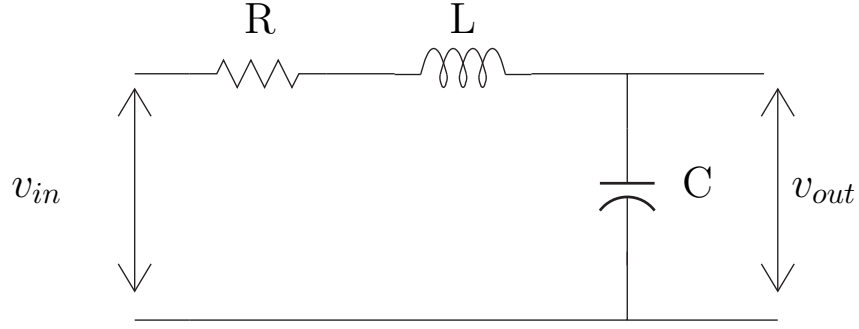


FIGURE 4.7. A RLC series circuit.

The transfer function  $v_{out}/v_{in}$  is given by,

$$\frac{v_{out}(s)}{v_{in}(s)} = \frac{\frac{1}{sC}}{\frac{1}{sC} + R + sL} \quad (4.40)$$

Rearranging we get,

$$\frac{v_{out}(s)}{v_{in}(s)} = \frac{\frac{1}{LC}}{s^2 + s\frac{R}{L} + \frac{1}{LC}} \quad (4.41)$$

Equation (4.41) has a frequency characteristic which is similar to the transfer function (4.3) that shapes the Brownian noise  $F_N$ . Let us assume that the  $R, L, C$  parameters are chosen in such a way that  $\frac{R}{L} = \frac{\omega_n}{Q_M}$  and  $\omega_n^2 = \frac{1}{LC}$ . Substituting the relations in (4.41),

$$\frac{v_{out}(s)}{v_{in}(s)} = \frac{\omega_n^2}{s^2 + s\frac{\omega_n}{Q_M} + \omega_n^2} \quad (4.42)$$

Substituting  $s = j\omega$  in (4.42) and squaring the magnitude,

$$\left| \frac{v_{out}(\omega)}{v_{in}(\omega)} \right|^2 = \left| \frac{\omega_n^2}{s^2 + s\frac{\omega_n}{Q_M} + \omega_n^2} \Big|_{s=j\omega} \right|^2 \quad (4.43)$$

$$= \frac{\omega_n^4}{(\omega_n^2 - \omega^2)^2 + \left(\frac{\omega_n\omega}{Q_M}\right)^2} \quad (4.44)$$

Rearranging the squared transfer function we get,

$$\left| \frac{v_{out}(\omega)}{v_{in}(\omega)} \right|^2 = \frac{1}{\left[ \left(1 - \frac{\omega^2}{\omega_n^2}\right)^2 + \frac{1}{Q_M^2} \frac{\omega^2}{\omega_n^2} \right]} \quad (4.45)$$

The above expression captures the frequency characteristics of the displacement noise power spectral density. Comparing Eqs. (4.45) and (4.5), we find that they differ by a constant factor given by  $C_{cons} = \frac{4k_B T r}{k^2}$ . This factor is same as that of thermal noise in a resistor with an equivalent resistance given by  $R_{eq} = \frac{r}{k^2}$ . Hence, the displacement noise power spectral density can be modeled as a thermal noise source shaped by the transfer function given by (4.45). Figure 4.8 shows the equivalent circuit to model the displacement noise in MEMS varactors. The noise voltage across  $R_{eq}$  is given as an input to the noise shaping RLC series circuit through a voltage controlled voltage source (VCVS) with unity gain. It should be noted that the resistor  $R$  in the noise shaping RLC series circuit is made noiseless for simulation purposes.

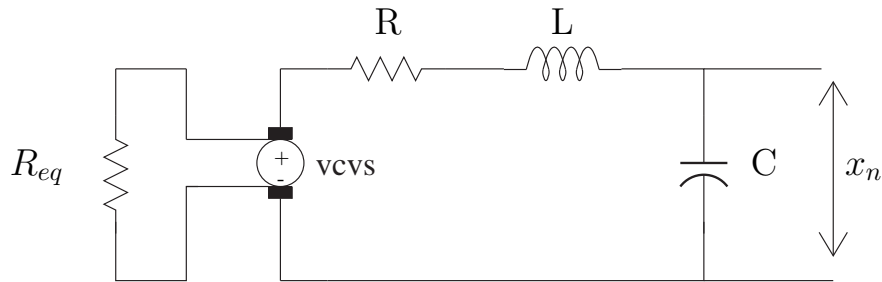


FIGURE 4.8. Equivalent circuit to model the displacement noise.

This equivalent circuit model can be added to the behavioral model described in Section 2.3.2 to account for the mechanical noise in the MEMS varactor. Figure 4.9 shows how the equivalent circuit model can be used along with the AHDL behavioral model to account for the mechanical noise. The output of the equivalent circuit model has a noisy component of current due to the injected noise voltage  $x_n(t)$ . It can be easily verified that this noise component of current has a power spectral density which is the same as  $\overline{i_{n1}^2(\omega)}$  in (4.29). Figure 4.9 shows that simulated output noise from the equivalent circuit model matches well with the analytical expression in (4.29).

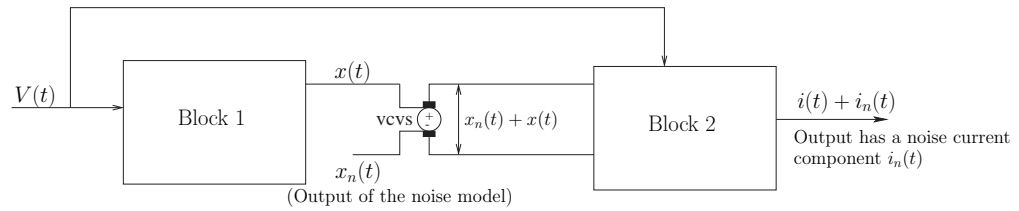


FIGURE 4.9. Behavioral-circuit model.

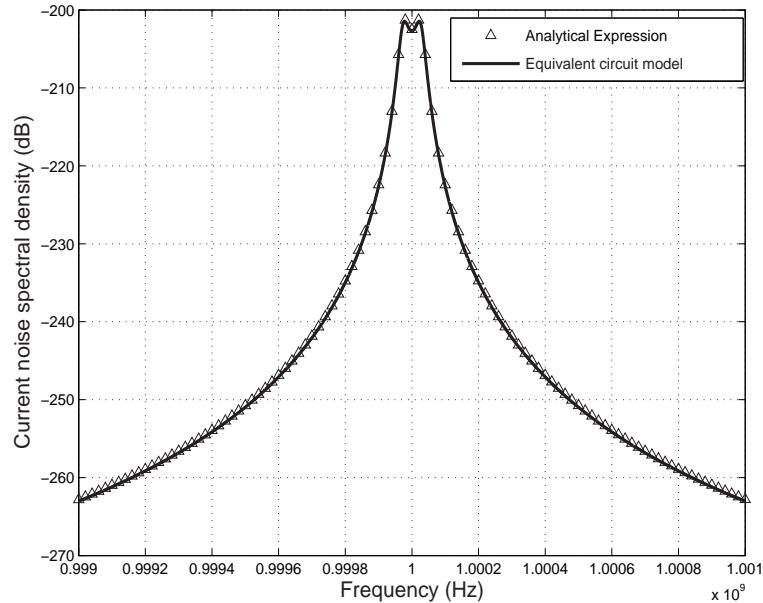


FIGURE 4.10. Output current noise of the equivalent circuit model.

#### 4.7. Simulation Results

Phase noise simulations were performed on an 800 MHz single-ended Colpitts VCO implemented in a HP 0.8  $\mu\text{m}$  CMOS technology, using the techniques and models described in the previous sections. The Colpitts VCO as shown in Figure 4.11 uses four identical MEMS variable capacitors each with an overlap area of 200  $\mu\text{m}$  x 200  $\mu\text{m}$  and an air-gap of 1.5  $\mu\text{m}$ . The different simulation approaches used to evaluate the phase noise contribution of the MEMS capacitors are described as follows.

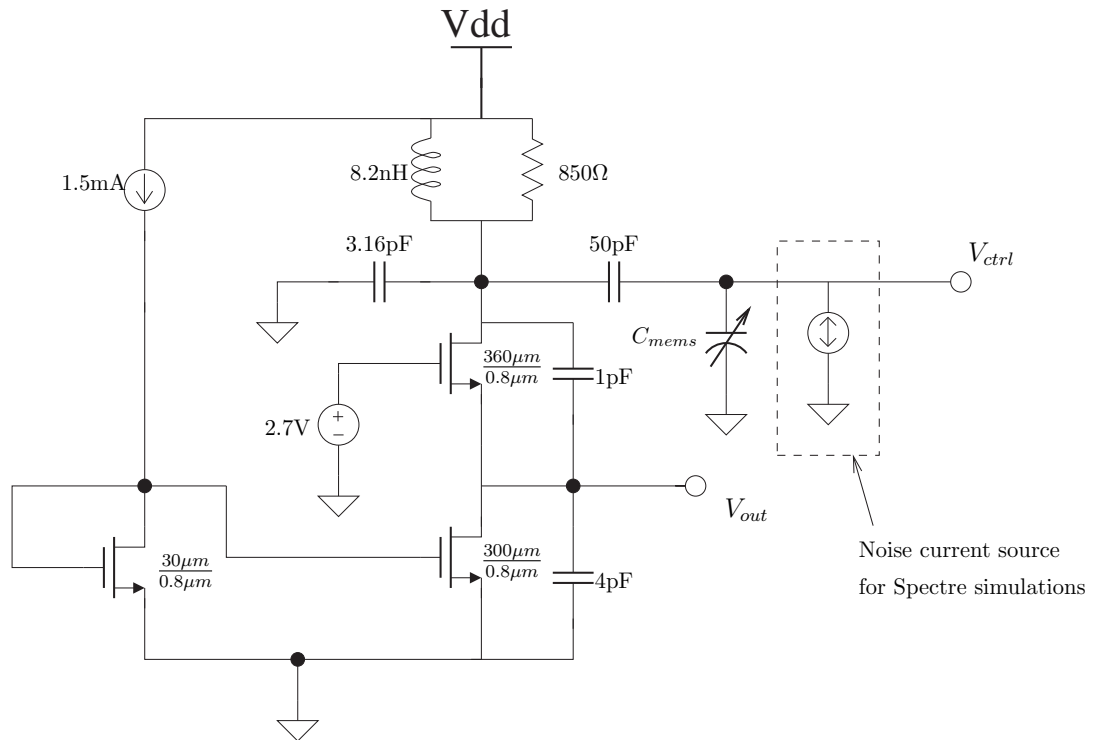


FIGURE 4.11. Colpitts VCO.

- (1) *Proposed technique* : In Section 4.5, a simulation technique to evaluate the Brownian motion induced phase noise using the non linear perturbation analysis, was proposed. The proposed technique uses the non-linear perturbation analysis implemented in SPICE3f5 [20] for phase noise computation. Eqs. (4.38) and (4.39) were used to evaluate the noise contribution of the MEMS capacitors.
- (2) *Spectre simulations using current noise source* : Phase noise simulations of the Colpitts VCO were performed using the Spectre Pnoise analysis. A noise current source with a power spectral density that is the same as  $\overline{i_{n1}^2(\omega)}$  is used to model the mechanical noise in MEMS capacitors. Figure 4.11 illustrates the simulation setup. This simulation basically injects the current

noise power spectrum (4.29) of the MEMS capacitor, into the oscillator and observes the resultant phase noise. For phase noise simulation, this approach uses a noise file with values computed using Eq. (4.29). Eq. (4.29) is derived based on the assumption that the voltage across the MEMS capacitor is a pure sinusoid. The Colpitts oscillator in Figure 4.11 has very low distortion and hence the oscillation waveform is close to a pure sinusoidal signal. We use this method for validating the simulation techniques (1) and (4).

- (3) *Noise behavioral model simulations* : This technique uses the noise model shown in Figure 4.4, to inject the current noise power spectrum into the oscillator. The noise model was implemented in SpectreHDL and phase noise simulations were performed using the Spectre Pnoise analysis. This simulation was performed to show that technique (2) is consistent with the noise analysis presented in Section 4.4.1.
- (4) *Equivalent circuit model* : In Figure 4.9, a high-level model for MEMS varactors that takes into account the mechanical noise was presented. Spectre simulations were performed using the model to compute the phase noise.

Figure 4.12 shows phase noise results using the different simulation approaches. They show similar trends and match the theoretical phase noise profile shown in Figure 4.2. The different simulation approaches agree well with each other. The simulation techniques (2) and (3) validate the phase noise simulations using the proposed technique and the equivalent circuit model.

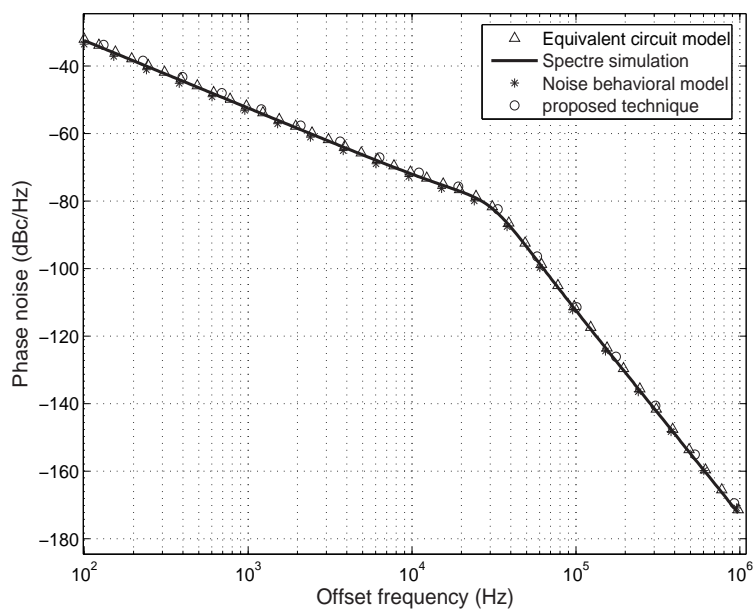


FIGURE 4.12. Phase noise computed using different simulation approaches

$Q_M=1$ .

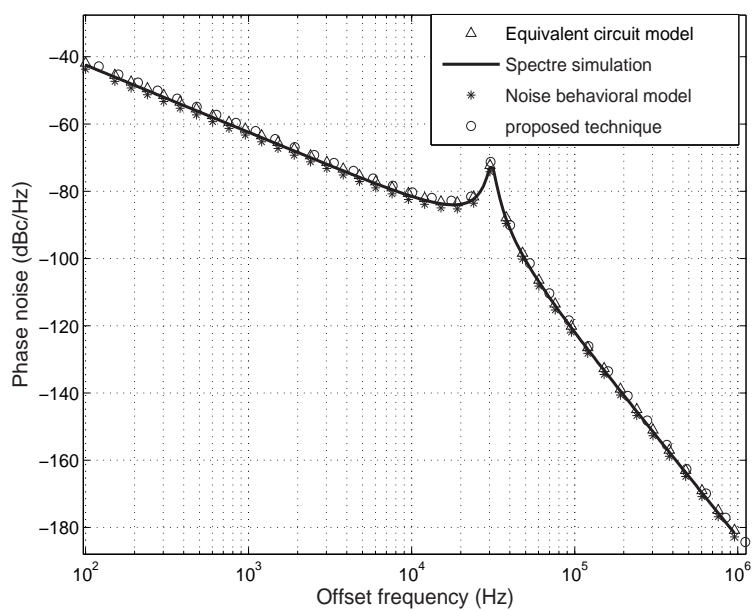


FIGURE 4.13. Phase noise computed using different simulation approaches for

$Q_M=10$ .

## 4.8. Summary

A phase noise simulation technique to account for the mechanical noise in MEMS varactors is discussed in this chapter. The Brownian noise in MEMS varactors is modeled as an equivalent noise current source in the electrical domain. A detailed mathematical analysis is used to derive the power spectral density of the current noise source. Based on the analysis, it was found that the equivalent current noise is cyclostationary in nature. Considering that the output noise of an oscillator is a stationary process, [17], [18], only the time average power spectral density of the current noise is accounted for in the phase noise analysis. Finally, an equivalent circuit model that can be used along with the behavioral model to account for the Brownian noise is presented. Simulations using the proposed simulation technique, and the equivalent circuit model are in good agreement with simulations in Spectre.

## 5. CONCLUSIONS AND FUTURE WORK

This work has explored the application of coupled simulation techniques and high-level models for the simulation of RF MEMS VCOs. A circuit model and a behavioral model for MEMS based varactors are discussed and their accuracy issues are identified, based on comparisons with numerical simulations. A faster simulation technique based on the time-domain shooting method is proposed for the computation of the periodic steady state in oscillators. This method exploits the dynamic behavior of MEMS based varactors to reduce the number of device calls and improve the simulation time. A phase noise analysis technique to account for the mechanical noise in MEMS varactors is presented. In order to account for the mechanical noise in high-level models, an equivalent circuit to model the Brownian noise is developed.

Much work remains to be done in the phase noise simulation of RF MEMS VCOs. The phase noise analysis technique presented in this work is applicable for two parallel plate MEMS capacitors. The same approach can be extended for cantilever and fixed-fixed beams. Numerical simulations of MEMS based varactors involve discretizing the surface of the beams into distinct nodes. In case of the cantilever and fixed-fixed beams, each of these discrete elements can be modeled as a parallel plate capacitor. Hence, the proposed simulation technique can be used for each of these discrete elements to compute the overall phase noise.

## BIBLIOGRAPHY

- [1] B. Razavi, "Challenges in portable RF transceiver design," *IEEE Circuits and Devices Mag.*, vol. 12, pp. 12-25, Sept. 1996.
- [2] P. R. Gray and R. G. Meyer, "Future directions in silicon ICs for RF personal communications," in *Proc. IEEE Custom Integrated Circuits Conf.*, May 1995, pp. 83-90.
- [3] D. J. Young, "Micromechanical Devices and Fabrication Technologies for Radio-Frequency Analog Signal Processing," *Ph.D. Dissertation*, Univ. of California, Berkeley, 1999.
- [4] S. D. Senturia, R. M. Harris, B. P. Johnson, S. Kim, K. Nabors, M. A. Shulman, and J. K. White, "A computer-aided design system for microelectromechanical systems (MEMCAD)," *IEEE J. Microelectromech. Syst.*, vol. 1, pp. 3-13, Mar. 1992.
- [5] R. M. Kirby, G. E. Karniadakis, O. Mikulchenko, and K. Mayaram, "An integrated simulator for coupled domain problems in MEMS," *IEEE J. Microelectromech. Syst.*, vol. 10, pp. 379-391, Sept. 2001.
- [6] M. Behera, "Coupled Circuit and Device Simulations for Design of RF MEMS VCOs," *M.S. Thesis*, Oregon State University, May 2004.
- [7] D. Young and B. E. Boser, "A micromachined-based RF low noise voltage controlled oscillator," in *Proc. IEEE Custom Integrated Circuits Conf.*, May 1997, pp. 431-434.
- [8] A. Dec and K. Suyama, "Micromachined electromechanically tunable capacitors and their applications to RF ICs," *IEEE Trans. Microwave Theory Tech.*, vol. 46, pp. 2587-2595, Dec. 1998.
- [9] A. Dec and K. Suyama, "Microwave MEMS-based voltage controlled oscillators," *IEEE Trans. Microwave Theory Tech.*, vol. 48, pp. 1943-1949, Nov. 2000.
- [10] G. Li and N. R. Aluru, "Efficient mixed-domain analysis of electrostatic MEMS," in *IEEE/ACM International Conference on Computer-Aided Design*, Nov. 2004, pp. 474-477.
- [11] G. M. Rebeiz, *RF MEMS Theory, Design and Technology*, John Wiley and Sons, 2003.

- [12] M. Behera, S. De, N. Aluru and K. Mayaram, "A coupled circuit and device simulator for design of RF MEMS VCOs," in *IEEE-Nano Conf.*, vol. 2, Aug. 2003, pp. 347-350.
- [13] K. Kundert, "Introduction to RF simulation and its applications," *IEEE J. Solid-State Circuits*, vol. 34, pp. 1298-1319, Sept. 1999.
- [14] K. Mayaram, D. C. Lee, S. Moinian, D. A. Rich, and J. Roychowdhury, "Computer-aided circuit analysis tools for RFIC simulation: algorithms, features, and limitations," *IEEE Trans. CAS-II*, pp. 274-286, April 2000.
- [15] A. Demir, "Analysis and Simulation of Noise in Nonlinear Electronic circuits and Systems," *Ph.D. Dissertation*, Univ. of California, Berkeley, 1997.
- [16] W. A. Gardner, *Introduction to Random Processes with Applications to Signals and Systems*, McGraw-Hill, second Edition, 1990.
- [17] A. Demir, A. Mehrotra, and J. Roychowdhury, "Phase noise in oscillators: a unifying theory and numerical methods for characterization," *IEEE Trans. Circuit Syst.-I*, vol. 47, pp. 655-674, May 2000.
- [18] A. Demir, "Phase noise in oscillators: DAEs and colored noise sources," in *Proc. IEEE/ACM International Conference on Computer-Aided Design*, Nov. 1998, pp. 170-177.
- [19] J. Roychowdhury, D. Long, and P. Feldmann, "Cyclostationary noise analysis of large RF circuits with multi-tone excitations," *IEEE J. Solid-State Circuits*, vol. 33, pp. 324-336, Mar. 1998.
- [20] V. Kratyuk, "Algorithms and Tools for Optimization of Integrated RF VCOs," *M.S. Thesis*, Oregon State University, June 2003.

## APPENDICES

## APPENDIX A. AHDL code

### A.1. AHDL code for MEMS capacitor

```
// Spectre AHDL for ahdlmemsmodel, block1
module block1 ( xn, xp, vn, vp) (epi,A,d1,m,r,k,kb,T)
    node [V,I] xn;
    node [V,I] xp;
    node [V,I] vn;
    node [V,I] vp;
parameter real epi = 0.0000000000088589312;
parameter real A=0.000000040000;
parameter real d1 = 0.00000150;
parameter real m =0.0000000001;
parameter real r=0.00002/10;
parameter real k = 3.8;
parameter real kb=1.32e-23;
parameter real T=300;
{
node [V,I] tem;
analog {
V(tem) <- dot(V(xp,xn));
V(xp, xn) <- -0.5*epi*A*V(vp,vn)*V(vp,vn)/(k*(d1 + V(xp,xn))*(d1 +
V(xp,xn))) - m*dot(V(tem))/k - r*V(tem)/k ;
}
}

// Spectre AHDL for ahdlmemsmodel, block2, ahdl
module block2 ( outn, outp, vinn, vinp, xinn, xinp)
(epi,A,d1,m,r,k)
    node [V,I] outn;
    node [V,I] outp;
    node [V,I] vinn;
    node [V,I] vinp;
    node [V,I] xinn;
    node [V,I] xinp;
parameter real epi = 0.0000000000088589312;
parameter real A =0.000000040000;
parameter real d1 = 0.00000150;
parameter real m =0.0000000001;
parameter real r = 0.00002/10;
parameter real k =3.8;
```

```

{
node [V,I] temv; node [V,I] temx;
analog {
V(temv) <-dot(V(vinp,vinn))*0.000000001;
V(temx) <- dot(V(xinp,xinn));
I(outp,outn) <- epi*A*V(temv)*1e9/(V(xinp,xinn)+d1) +
                epi*A*V(vinp,vinn)*V(temx)/((V(xinp,xinn)+d1)*(V(xinp,xinn)+d1));
}
}

```

## A.2. AHDL code for noise behavioral model

```

// Spectre AHDL for RLC series circuit
//AHDL Code to model the equivalent circuit noise model

module white_noi(outn, outp) (kb, T, r, k)
    node [V,I] outn;
    node [V,I] outp;
parameter real kb = 1.32e-23;
parameter real T = 300;
parameter real r =1.95e-6 ;
parameter real k=3.8;
{
node [V,I]
temv,diff;
analog {
V(outp,outn) <- $white_noise( 4*kb*T*r/(k*k) , "source1" );
}
}

// Spectre AHDL to model Brownian noise

module white_noi(outn, outp) (kb, T, r, k)
    node [V,I] outn;
    node [V,I] outp;
    parameter real kb = 1.32e-23;
parameter real T = 300;
parameter real r =1.95e-6 ;
parameter real k=3.8;
{
    node [V,I] temv,diff;

```

```

    analog {
V(outp,outn) <- $white_noise( 4*kb*T*r/(k*k) , "source1" );
}
}

// Spectre AHDL code for the periodic modulation
//in the noise model
module block2 ( outn, outp, vinn, vinp, xinn, xinp)
(epi,A,d1,m,r,k)
    node [V,I] outn;
    node [V,I] outp;
    node [V,I] vinn;
    node [V,I] vinp;
    node [V,I] xinn;
    node [V,I] xinp;
parameter real epi = 0.0000000000088589312;
parameter real A =0.000000040000;
parameter real d1 = 0.00000150;
parameter real m =0.0000000001;
parameter real r = 0.00002/10;
parameter real k =3.8;
{
node [V,I] temv;
node [V,I] temx;
analog {
    V(temv)<-dot(V(vinp,vinn))*0.000000001;
    V(temx) <- dot(V(xinp,xinn));
    I(outp,outn) <- epi*A*V(temv)*1e9/(V(xinp,xinn)+d1);
}
}
}

```

## APPENDIX B. Spice netlist

### B.1. MEMS equivalent circuit model

```

*mems equivalent circuit model-HSpice netlist

.op
.options post  CAPTAB numdgts=10 vabstol=1e-15
v1 4 0 sin(0 1 1e9)

```

```

*VCCS for electrostatic force
gin 1 0 CUR='0.5*8.8541e-12*230*230*v(4,0)*v(4,0)/((v(6,0)-0.75)*
(v(6,0)-0.75))'

*mass as capacitor
c1 1 0 0.6e-9

*damping as conductance
rq 1 0 6.84e3

*integrator
gin2 2 0 1 0 1e-6
c2 2 0 1e-6
r2 2 0 100T

e6 6 0 vcvs 2 0 1e6

*Restoring force as VCCS
gin3 0 1 POLY(1) 2 0 0 44

*Current components in MEMS capacitor
c3 4 0 C='8.8541e-12*230*230e-6/(0.75-v(6,0))' CTYPE=1
gin4 0 4 CUR='8.8541e-12*230*230*v(1,0)*v(4,0)/((v(6,0)-0.75)*(v(6,0)-0.75))'

.tran 0.01n 50u
.plot tran v(6,0)
.print tran v(6,0)
.end

```

## B.2. Colpitts Oscillator

```

* colpitts oscillator

vdd vdd 0 3.3
Lb vdd 1 8.2n ic=1m
Rp vdd 1 850
Cp 1 0 3.16p
Cdum 1 ctrl 1u
Rdum ctrl 0 1e6
n1 ctrl 0 Nx w=200u l=200u dg=1.5u
n2 ctrl 0 Nx w=200u l=200u dg=1.5u

```

```

n3 ctrl 0 Nx w=200u l=200u dg=1.5u
n4 ctrl 0 Nx w=200u l=200u dg=1.5u
M1 1 2 out 0 cmosn w=360u l=0.8u ad=864p as=864p pd=724.8u
ps=724.8u
M2 out 3 0 0 cmosn w=300u l=0.8u ad=720p as=720p
pd=604.8u ps=604.8u
M3 3 3 0 0 cmosn w=30u l=0.8u ad=72p as=72p
pd=148.8u ps=148.8u
C1 1 out 1p
C2 out 0 4p
Ibias vdd 3 1.5m vbias 2 0 2.7
.op
.options post reltol=1e-4 vabstol=1e-7 iabstol=1e-13
gmin=1e-13 rforce=1
.model Nx N simtype=2 capttype=2 qm=15 pullin=10 km=3.4
mass=2.15e-10 tstep=0.01n +tpxelem=81 tpyelem=5 bpxelem=81
bpyelem=5 tpthick=1u bpthick=1u
.tran 1n 20u 0 100p UIC
.pnoise v(out) 721Meg 100 10Meg dec 10 15
.print tran v(out)
.end

```

### B.3. LC Oscillator

```

*LC oscillator

vdd 1 0 2.7
l1 1 2 3.84n IC=1m
rp1 1 2 325.2
l2 1 3 3.84n
rp2 1 3 325.2
cp1 2 4 0.6p
cp2 3 4 0.6p
n1 2 4 Nx w=295u l=295u dg=0.75u
n2 3 4 Nx w=295u l=295u dg=0.75u
vctrl 4 0 2.4
M1 2 3 5 0 n w=100u l=1u ad=132p as=132p pd=222.4u ps=222.4u
M2 3 2 6 0 n w=100u l=1u ad=132p as=132p pd=222.4u ps=222.4u
cc 5 6 10p
ld1 5 7 10n ld2 6 8 10n
rd1 7 0 390 rd2 8 0 390

```

```
c10 7 0 35p c20 8 0 35p
.op
.steady act auto 0.625e-9 100 1e-6 uic 1
.print steady v(2)
.model Nx N simtype=3 capttype=3 tstep=0.1e-6 qm=10 +
maxiter=10 pullin=3.3
```

